MODE AND SAWTOOTH BEHAVIOUR DURING NEUTRAL BEAM INJECTION IN THE W VII-A STELLARATOR

W VII-A Team

IPP 2/250 February 1980

MAX-PLANCK-INSTITUT FÜR PLASMAPHYSIK

8046 GARCHING BEI MÜNCHEN

MAX-PLANCK-INSTITUT FÜR PLASMAPHYSIK

GARCHING BEI MÜNCHEN

MODE AND SAWTOOTH BEHAVIOUR DURING NEUTRAL BEAM INJECTION IN THE W VII-A STELLARATOR

W VII-A Team

IPP 2/250 February 1980

Die nachstehende Arbeit wurde im Rahmen des Vertrages zwischen dem Max-Planck-Institut für Plasmaphysik und der Europäischen Atomgemeinschaft über die Zusammenarbeit auf dem Gebiete der Plasmaphysik durchgeführt.

W VII-A TEAM

- Project leaders	G. Grieger H. Renner J. Sapper H. Wobig
- Running of the experiment	D. Dorst H. Renner J. Sapper
- Theory	H. Wobig G. Cattanei P. Javel F. Rau
- Electronics workshop	M. Zippe

DIAGNOSTICS

- Basic plasma parameters	H. Renner
- Bolometry	H. Jäckel
- Charge exchange	J. Junker
- Data acquisition	R. Lathe
- Doppler broadening - UV and visible spectroscopy	W. Ohlendorf
- Electron cyclotron emission	D. Bartlett^{++} M. Tutter B. Ulrich^{++}
- H-α emission	H. Ringler
- Infrared scattering	C. Mahn R. Meyer^{++}
- Interferometry	E. Würsching
- Langmuir/HF probes	G. Müller
- Limiter	F. Rau
- Microwave scattering	J. How^{++}
- Mirnov - oscillations	R. Jaenicke
- Thomson scattering	S. Marlier H. Ringler
- VUV spectroscopy	H. Hacker
- X-ray emission	P. Smeulders A. Weller

NEUTRAL INJECTION TEAM

(Technology Division)

- Numerical computations	J. Lister[++]
- Experiments	W. Ott E. Speth
- Technical systems	D. Cooper[++] R. Freudenberger

[++] Guest scientists

IPP 2/250

W VII-A Team

Mode and Sawtooth Behaviour During Neutral Beam Injection in the W VII-A Stellarator

Februar 1980 (in English)

ABSTRACT

The mode behaviour during Neutral Beam Injection in the WENDELSTEIN VII-A stellarator is presented. The analysis is mainly relying on soft X-ray measurements.

Two types of discharges were found during Neutral Beam Injection with plasma currents $\geq$ 20 kA. The first type is dominated by large, regular and long sawteeth, which are caused by a (m,n)=(1,1) mode. In the second type the sawteeth disappear completely. Later in the discharge a local disruption causes a transition to the first type; this disruption has a (3,2) mode precursor. A new mode (2,2) is found and phase coupled to the (3,2) mode.

Even at a high external rotational transform (ι_0=0.23) a large (2,1) mode is found after the (3,2) mode has caused the local disruption.

At slightly lower ι_0 values major current disruptions may even occur. This is mainly due to the enhanced edge heating by the Neutral Beam Injection.

Results of simulations of the mode structures are also presented.

CONTENTS

1. INTRODUCTION

Two neutral beam injectors (30 kV, 30 A) /1/ have been in operation on the Wendelstein VII-A Stellarator (major radius R = 2.0 m, plasma radius $a \geq 0.10$ m; helical windings: $\ell = 2$, $m = 5$; shearless external rotational transform $t_o \leq 0.23$; main magnetic field $B_o < 4$ T). The neutral beam power, $P_b \leq 450$ kW, exceeds the ohmic power, $P_{OH} \sim 50$ to 100 kW, during neutral injection. The beams are co-injected horizontally at an angle of 84^o to the main magnetic field. Thus large losses due to particles trapped in the helical and toroidal mirrors are expected. Also the plasma radius is rather small, so that even at high plasma densities ($\bar{n}_e > 5 \cdot 10^{19} m^{-3}$) with $T_e(o) \sim 500$ eV full absorption of the injected beam is not achieved. It has been calculated /2/ that approximately 180 kW is actually absorbed in the plasma. This exceeds the ohmic power during neutral injection by a factor of three.

Furthermore a strong increase of the radiation level in the plasma centre has been observed, such that the radiation losses become a substantial part (~ 30 %) of the local input power (1 to 1.5 W/cm^3). Also a large increase (factor of 5) of the plasma beta during neutral injection is observed ($<\beta> \approx 10^{-3}$ and $\beta_\theta \sim 2$ during NI). Even more important is that the radial profile of the injected energy deposition is different to that of the ohmic power. This should be of influence on the current density radial profile. Indeed a substantial change in the mode activity and structure has been observed during neutral injection.

2. DIAGNOSTICS

The mode structure is analysed in the W VII-A device with the aid of the following diagnostics:

- Ultra-soft and soft X-ray detector arrays (USX- and SX-arrays) (in certain cases the local X-rays originating from runaway electrons impinging on the outer limiter can also be used),
- Magnetic measurements using sets of Mirnov coils,
- Electrical measurements using the four insulated limiter segments,
- H-α emissivity measurements with a set of photo-diodes focussed on different spatial positions in the limiter plane.

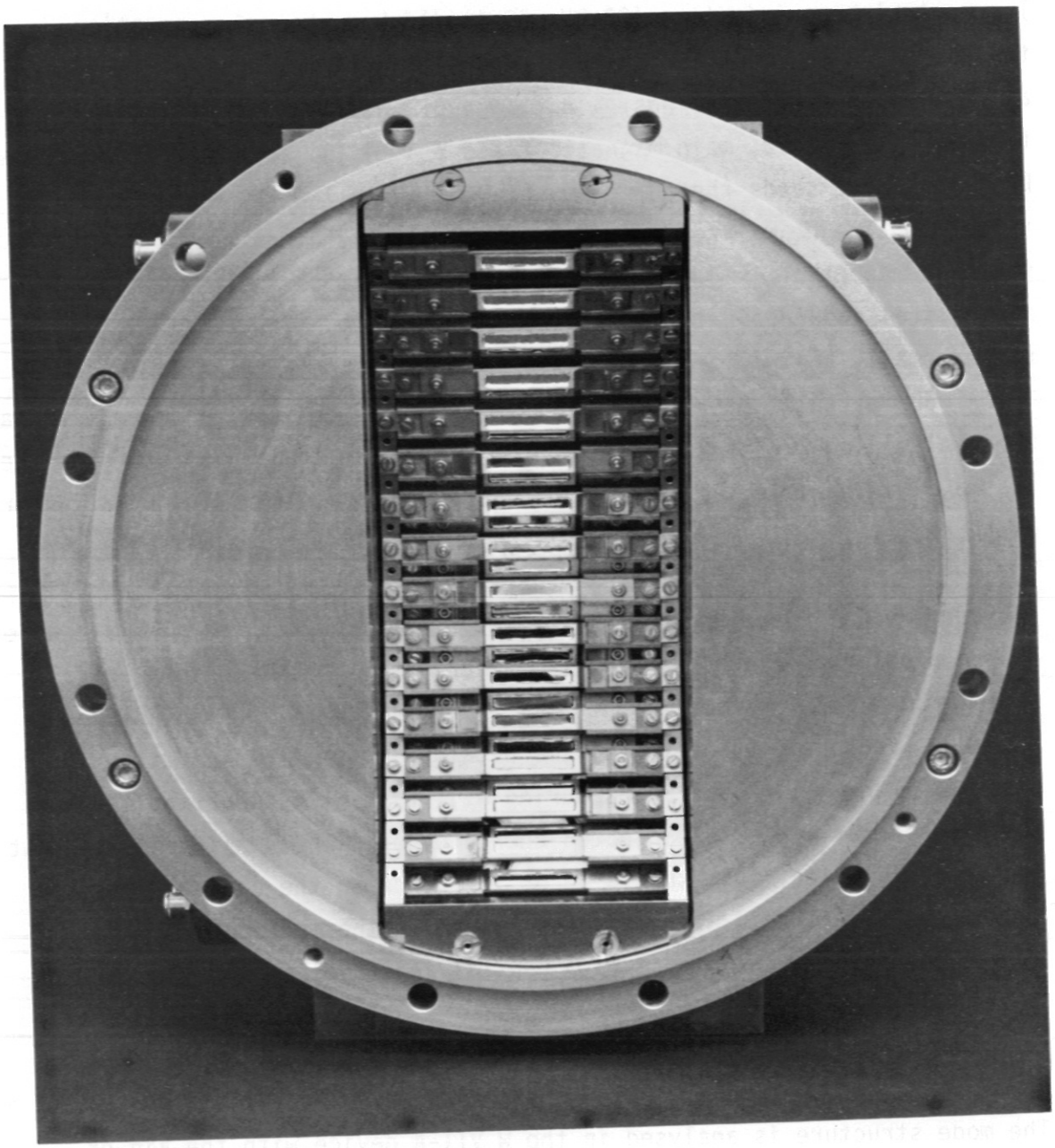

Fig. 1: The ultra soft X-ray diode array.

The ultra-soft X-ray detector array consists of 30 rectangular surface barrier diodes (Fig. 1), mounted in a high vacuum casing. The latter is connected to the torus vacuum by a small slit (Fig. 2). The spatial resolution obtained in this way is better than ≈ 1 cm in the plasma centre. With the 30 diodes the full poloidal aperture is viewed.

Thin beryllium filters of 0.5, 2.0, 25 and 75 μ thickness can be moved in front of the entrance slit in addition to the 0.1 μ thick aluminium window of the surface barrier diodes. A coarse energy resolution can thus be obtained. Table I shows the approximate energy bands for each filter combination.

	Filter	1st Band	2nd Band
	0.1 μ Al	15 eV < hν < 70 eV	250 eV < hν
II	+ 0.5 μ Be		350 eV < hν
III	+ 2 μ Be		570 eV < hν
IV	+ 25 μ Be		1400 eV < hν
	+ 75 μ Be		2000 eV < hν

TABLE I: Filter energy bands

The radial flux profiles obtained with the 30 diode array are Abel inverted /3/, taking into account the elliptical cross-section of the plasma /4/. At another toroidal position a set of two soft X-ray circular surface barrier detectors has been installed. These view the plasma at a radial position of ± 2.8 cm through a 25 μ thick beryllium window. The two detectors allow the toroidal mode number n of the instabilities near the plasma centre to be analysed (in particular the (m,n)=(1,1),(2,2) and (3,2) modes). Two large surface barrier diodes (with resp. a 328 and a 738 μ thick beryllium window) have been installed at the same position in order to determine the central electron temperature by the filter method /5/.

All the data obtained are stored on a PDP-11 computer via a CAMAC and CAMEM interface, built at the institute. The sampling time of the CAMAC interface is 1.2 μsec per channel so that with 4 channels per CAMAC unit, frequencies of 20 to 30 kcs can be readily detected. A total of 36 signals

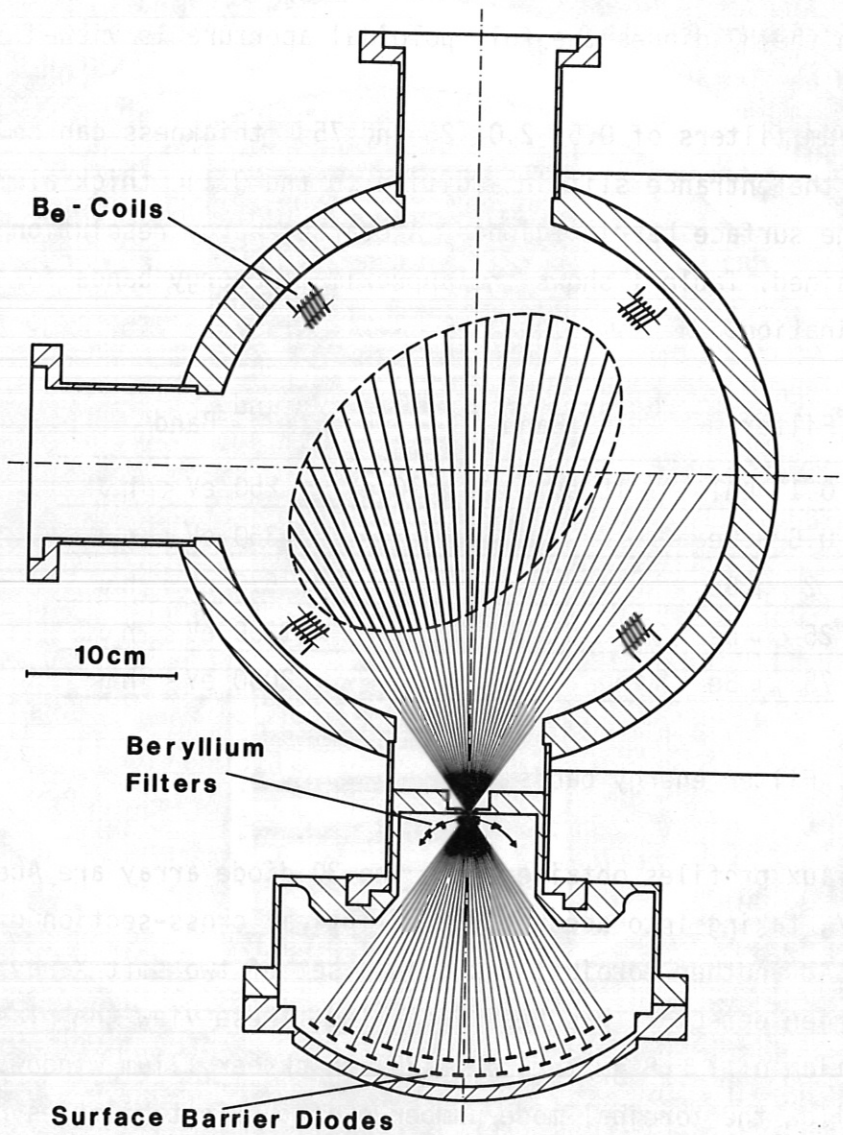

Fig. 2: Sketch of the ultra soft X-ray diode array.

each with 1 k 10-bits words are stored for each discharge. This, together with a variable amplification of a range of 1 to 1000, yields a dynamic range of $< 10^6$. Even this large dynamic range has sometimes proved to be too small during neutral injection.

The magnetic measurements are made outside the plasma, but inside the torus at three toroidal positions 108^o apart, with sets of 4 Mirnov coils equally spaces in the poloidal direction.

The different coils are combined together in such a way that the mode structure in poloidal (m-number) and toroidal (n-number) direction can be readily analysed. The signals are stored on fast transient recorders (200 kHz sampling rate, 8 bits and 1 k words). USX-array and magnetic signals are exchanged in order to make cross-relations.

3. MODE AND SAWTOOTH BEHAVIOUR DURING NEUTRAL BEAM INJECTION

In Wendelstein VII-A mode behaviour generally changes appreciably during neutral injection.

Two types of discharges have been observed for a plasma current of 20 kA and an external rotational transform ι_0 of 0.23 with the two available neutral injectors.

The first type is characterised by large regular internal sawtooth disruptions, which affect the energy confinement over more than half the plasma radius.

The second type is characterised by a disappearance of the regular sawteeth. This allows a further heating of the plasma centre, leading to the highest obtained central beta values.

Apparently the current density radial profiles are different for each type of discharge. This can also be seen from the position of the $q = 1$ surface. In the first type the $q = 1$ surface is at $r = 5$ cm, as seen from the position of the maximum of the (1,1) mode. (Fig. 4).

In the second type the q = 1 surface is at r = 3.5 cm, as seen from the position of the maximum of the (2,2) mode (Fig. 6). This mode is observed instead of the (1,1) mode. Coupling to the (3,2) mode due to the toroidal effect is probably responsible for the varied mode structure at the q = 1 surface. The increase in the sawtooth repetition time at the start of the neutral injection is qualitatively well understood from the increased edge heating and the increased central radiation losses due to the neutral beam injection as compared to the ohmic heating above.

In the first type of discharge the edge heating is apparently not sufficiently strong to prevent the current channel constriction, which leads to the internal sawtooth instability.

In the second type of discharge a small amount of deuterium has beed added to the helium discharge by gas puffing technique at the beginning of the neutral beam injection.

This apparently changes the energy deposition radial profile of the beams just sufficiently such that the sawtooth repetition time increases progressively and finally the sawtooth disruption seems to disappear.

In both types of discharges the level of the central radiation losses is roughly the same.

The second type of discharge usually turns over after a while to a sawtooth dominated discharge after one or more localised internal disruptions at the q = 1.5 surface. This leads in two ways to a cooling of the plasma centre, firstly by the internal disruption itself, secondly by the subsequent presence of large (1,1) and (2,1) modes.

These modes are destabilized by the change in the current density profile due to the internal disruption at the q = 1.5 surface.

Moreover the cooling of the plasma centre causes an increase of the power deposition from the neutral beams to the electrons in the centre. The change in the power deposition profile is probably the cause of the transition to a sawtooth dominated discharge.

B_o: 3.25 - 3.5 T

I_p: 17 - 25 kA

t_o: 0.17 - 0.23

t(a): 0.44 - 0.48

P_{OH}: 50 - 100 kW (120 - 180 kW)

P_{NI}(torus): 400-450 kW

P_{NI}(plasma): $\gtrsim$ 150 kW (calc.)

E_{dia} : 2.0 → 3.5 kJ
(0.5 to 1.0 kJ)

$\bar{\tau}_E$: 14 msec (calc. P_{NI})

$\bar{\beta}$: 10^{-3}

$T_e(o)$: 500 - 600 eV
(270 - 320 eV)

$n_e(o)$: 0.8 - 1.2 10^{14} cm^{-3}

Z_{eff} : 2 - 2.5

$P_{OH}(o)_{el}$: 0.4 - 0.7 W/cm^3
(1.1 - 1.4 W/cm^3)

$P_{NI}(o)_{el}$: 0.66 W/cm^3 (calc.)

$\tau_E(o)_{el}$: 13 msec
(3 - 5 msec)

$\beta(o) \sim 5\ 10^{-3}$
($\sim 10^{-3}$)

Table II: Plasma parameters in helium and helium/deuterium mixture with neutral injection. Values in brackets are without neutral injection.

At slightly lower values of the external rotational transform ι_o the (3,2) internal local disruption may even subsequentially lead to major current disruptions caused by very large (2,1) modes. These disruptions seems to be linked to a rather far inward location of the q = 2 surface.

An inward location can be achieved by
- a lower value of ι_o
- a lower plasma current
- and dynamically by an internal disruption at for instance the q = 1.5 surface.

This will be shown in the following chapters.

Plasma parameters for the neutral injection discharge are given in Table II. The values in brackets are for the target plasma without neutral beam injection.

4. FIRST TYPE DISCHARGES - INTERNAL SAWTOOTH DISRUPTIONS AT THE q = 1 SURFACE

Discharges with large, long, and regular sawtooth activity ($\Delta t_\nu \sim$ 5 msec, $\Delta T_e^\nu/T_e \sim 20$ %) are obtained when injecting two hydrogen beams of 450 kW total power into a helium plasma of density $< n_e > \sim 4$ to $5 \cdot 10^{13}$ cm^{-3}. The external rotational transform ι_o equals 0.23.

The sawteeth disruptions are characterised by large (1,1) percursors. A typical time evolution of the sawteeth is shown in Fig. 3 for ultra-soft X-ray fluxes with energies above 500 eV (through 2 μBe). Occasionally, in between the disruptions, a (3,2) mode of a constant amplitude appears.

The radial profile of the amplitude and phase of the (1,1) precursor is shown in Fig. 4. The asymmetry in the (1,1) mode amplitude is an indication of the presence of a small (2,1) mode, as is measured by the Mirnov coils.

The disruption causes a substantial loss of plasma energy and also a redistribution of the plasma current. The latter is straightforward to derive if one assumes that the effective plasma charge Z_{eff} does not change during the internal disruption. Since Z_{eff} is close to 2 (helium plasma) this assumption is reasonable. It is now possible to link the

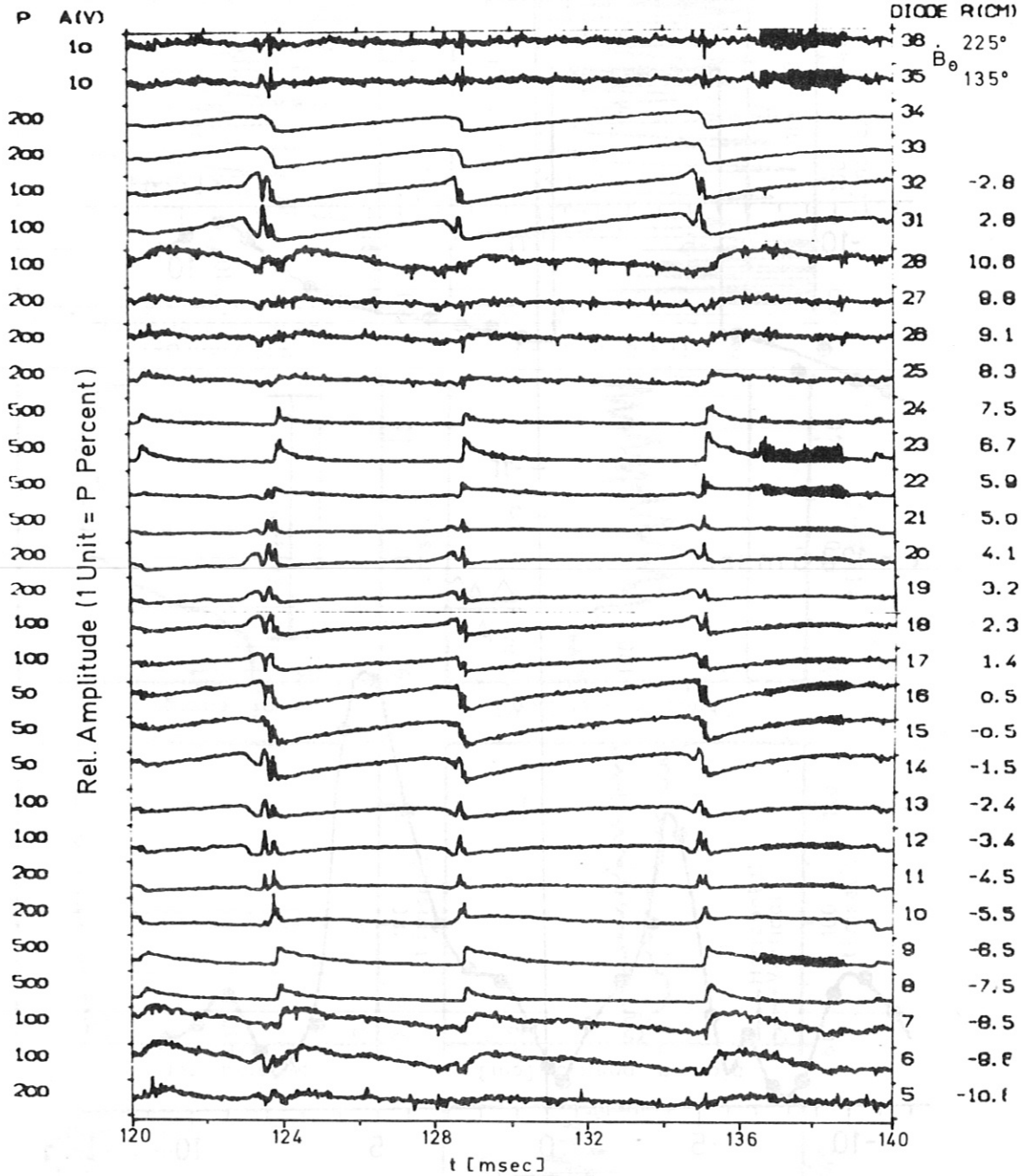

Fig. 3: Diode signals during (1,1) caused internal sawteeth, showing intermittent (3,2) mode activity (Shot: 19418, t_0=0.23, I_p=20 kA, 2 injectors, 2μBe); marked on the right is the normalised distance from each chord to the plasma centre, taking into account the plasma ellipticity.

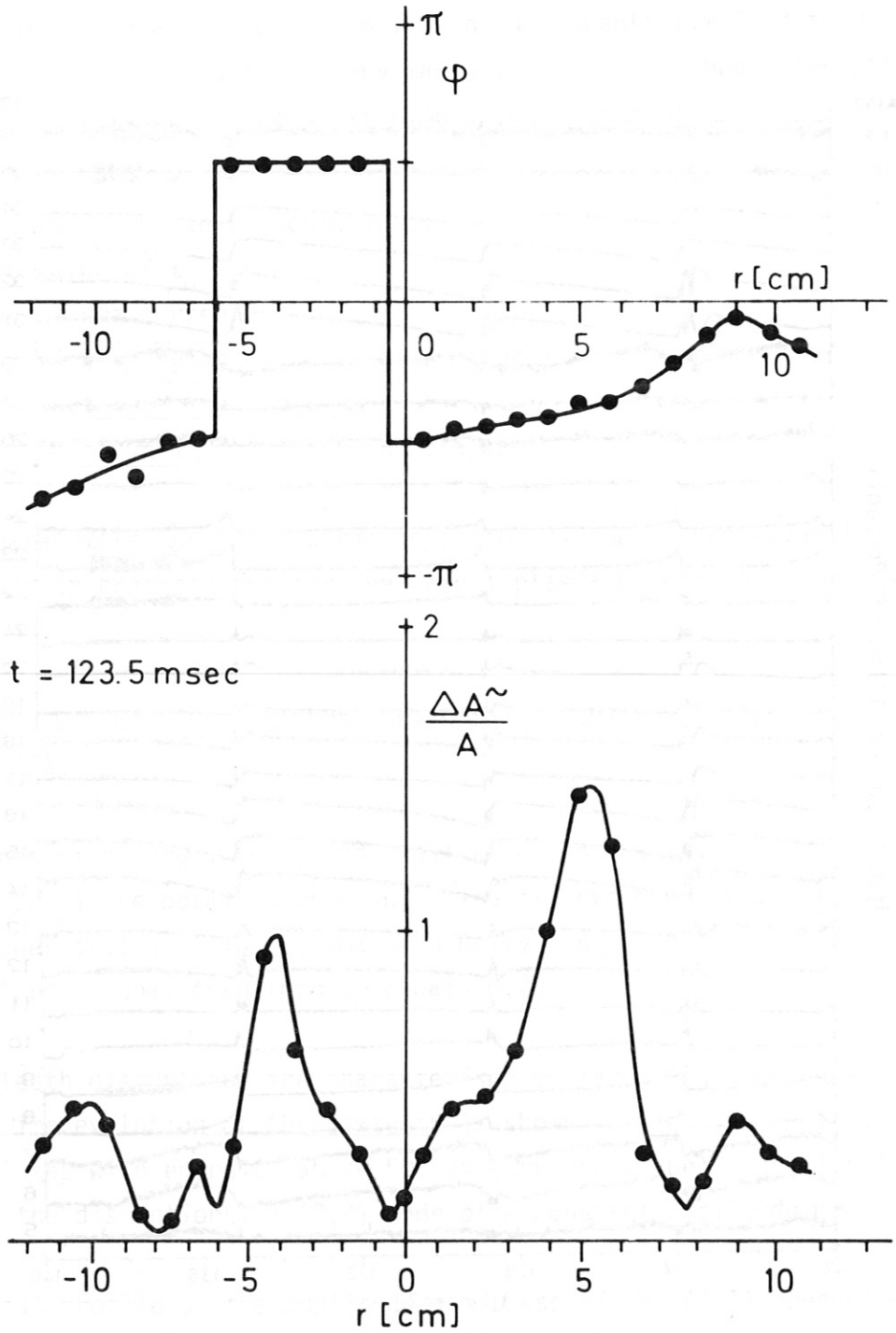

Fig. 4: Phase and relative amplitude radial profile of coupled (1,1) and (2,1) modes
(Shot: 19418, t_0=0.23, I_p=20 kA, 2 injectors, 2μBe).

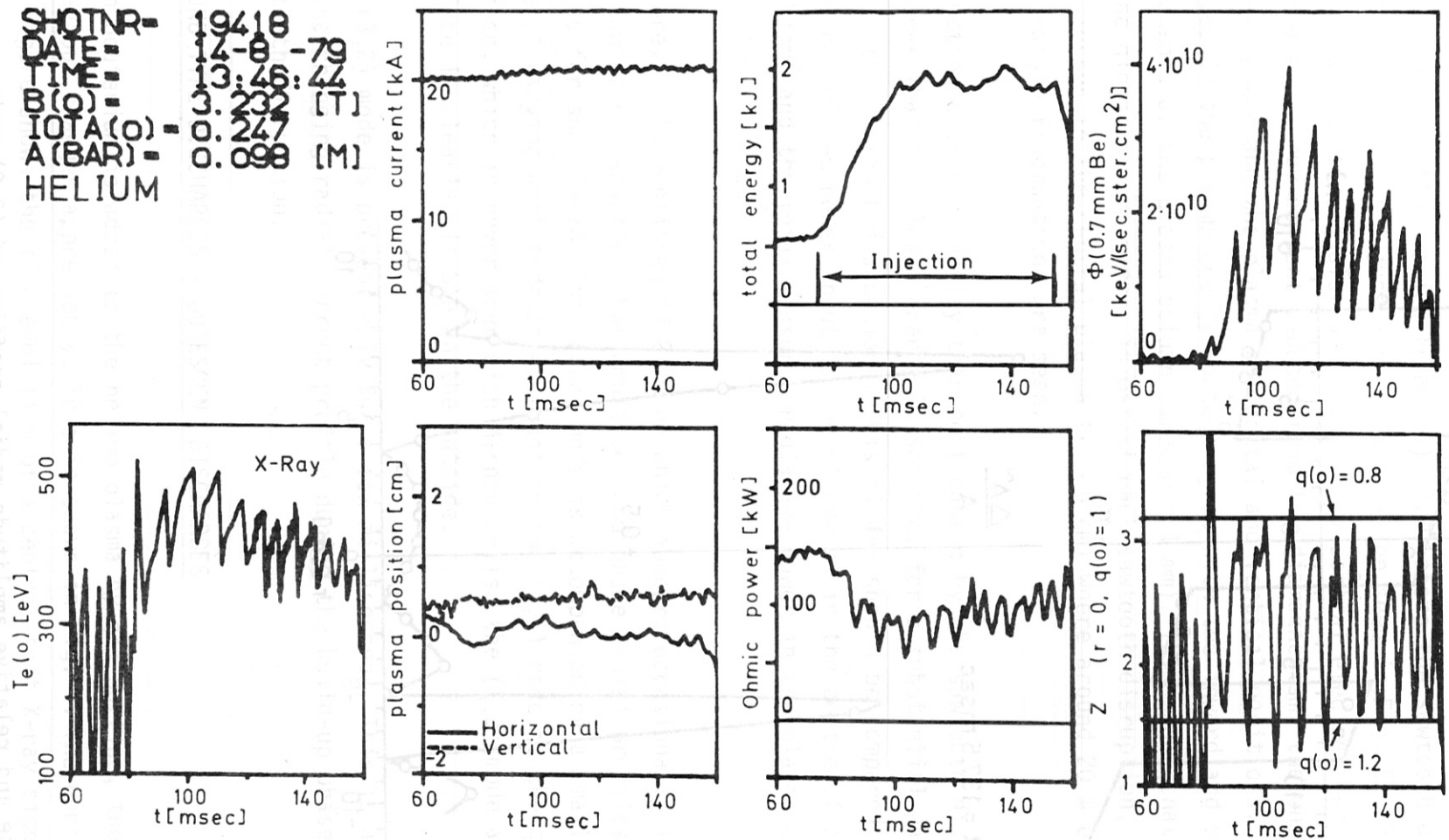

Fig. 5: Evolution of plasma parameters during Neutral Injection with large sawtooth (1,1) internal disruption.

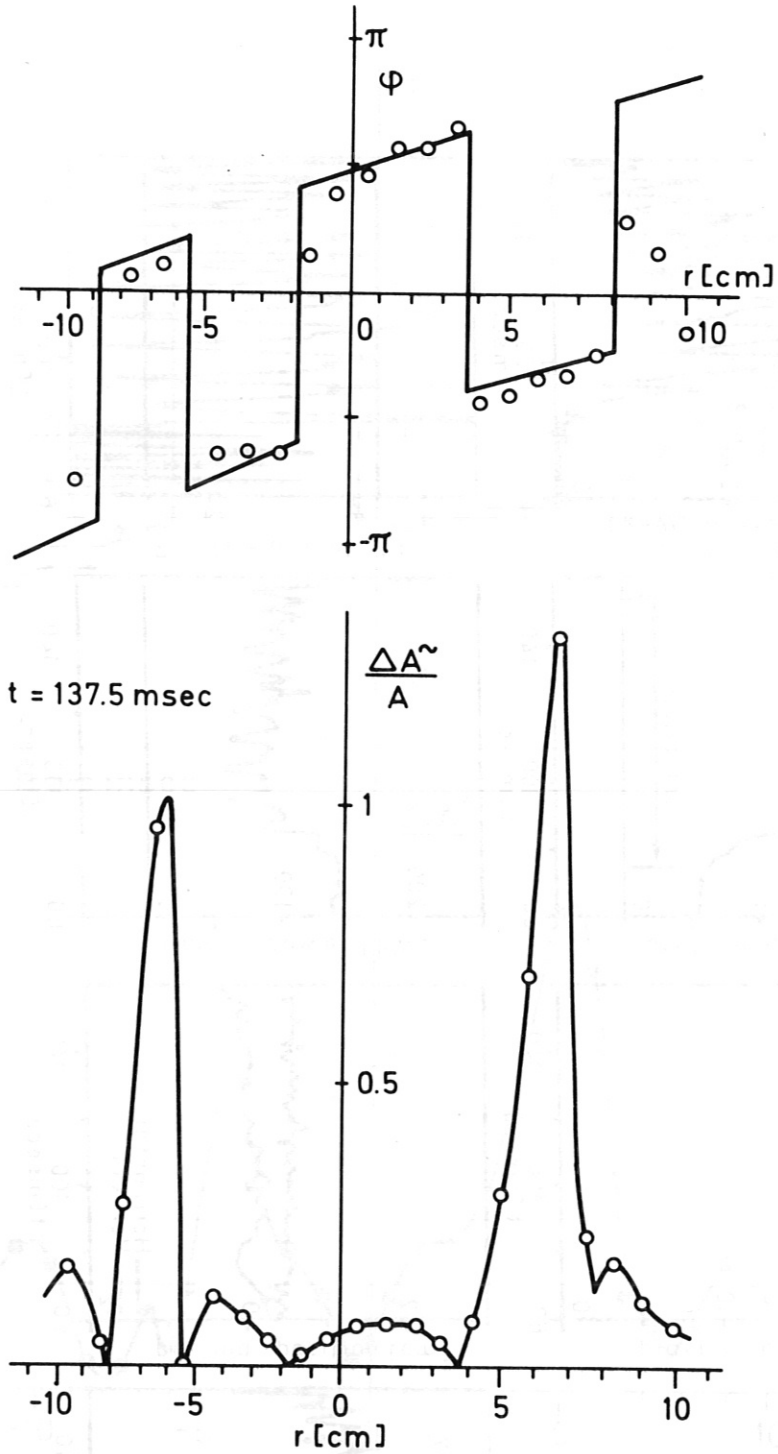

Fig. 6: Phase and relative amplitude radial profiles of (3,2) mode (Shot: 19418, t_o=0.23, I_p=20 kA, 2 injectors, 2μBe).

decrease in the resistive voltage, when the temperature drops (!) during the disruption, with a decrease in the central current density. Typically the change in the central current density is such that the central safety factor $q(o) = 1/t(o)$ varies from $q(o) \sim 0.8$ before the sawtooth disruption to $q(o) \sim 1.2$ just after. This can be seen in Fig. 5. The figure also shows the time evolution of the X-ray central electron temperature, the plasma energy content deduced from the diamagnetism, the ohmic heating power and the plasma horizontal and vertical positions. The changes in the plasma energy content agree with the inward and outward displacements of the plasma column (around ~ 1 mm). This shows that 7 to 8 % of the global plasma energy is lost at each sawtooth disruption, as compared with losses in the central plasma ($r \leq 5$ cm) where around 20 % electron temperature fluctuations are seen.

Neglecting electron density transport caused by the sawtooth disruptions, it is clear that the plasma energy losses are, for a substantial part (400 mW/cm^3), due to the sawtooth disruptions. This figure should be compared with the total calculated power input to the electrons in the centre of around ~ 1 W/cm^3 and the total measured radiative power in the plasma centre of ~ 300 to 500 mW/cm^3.

The previously mentioned (3,2) mode which appears occasionally inbetween the sawtooth disruptions has amplitude and phase radial profiles shown in Fig. 6 for shot 19418. This (3,2) mode is accompanied by a smaller (2,2) mode of varying amplitude.In contrast to the (1,1) mode at the q = 1 surface, which is never seen with Mirnov coils, the (2,2) mode at the same surface is clearly visible on the outside.

The (3,2) mode is present only for a few milliseconds. This is an indication of the changing radial current profile during the build-up phase of the sawteeth disruption.

5. SECOND TYPE DISCHARGES - QUIESCENT DISCHARGES

When deuterium is added to the helium plasma by gas puffing, the sawtooth behaviour changes appreciably. This is shown in Fig. 7. The upper part of the figure shows the time evolution of a central soft X-ray signal for a pure helium plasma. The neutral injection starts at ~ 75 ms. The increasing sawtooth period and subsequent decrease to ~ 5 msec can be clearly seen.

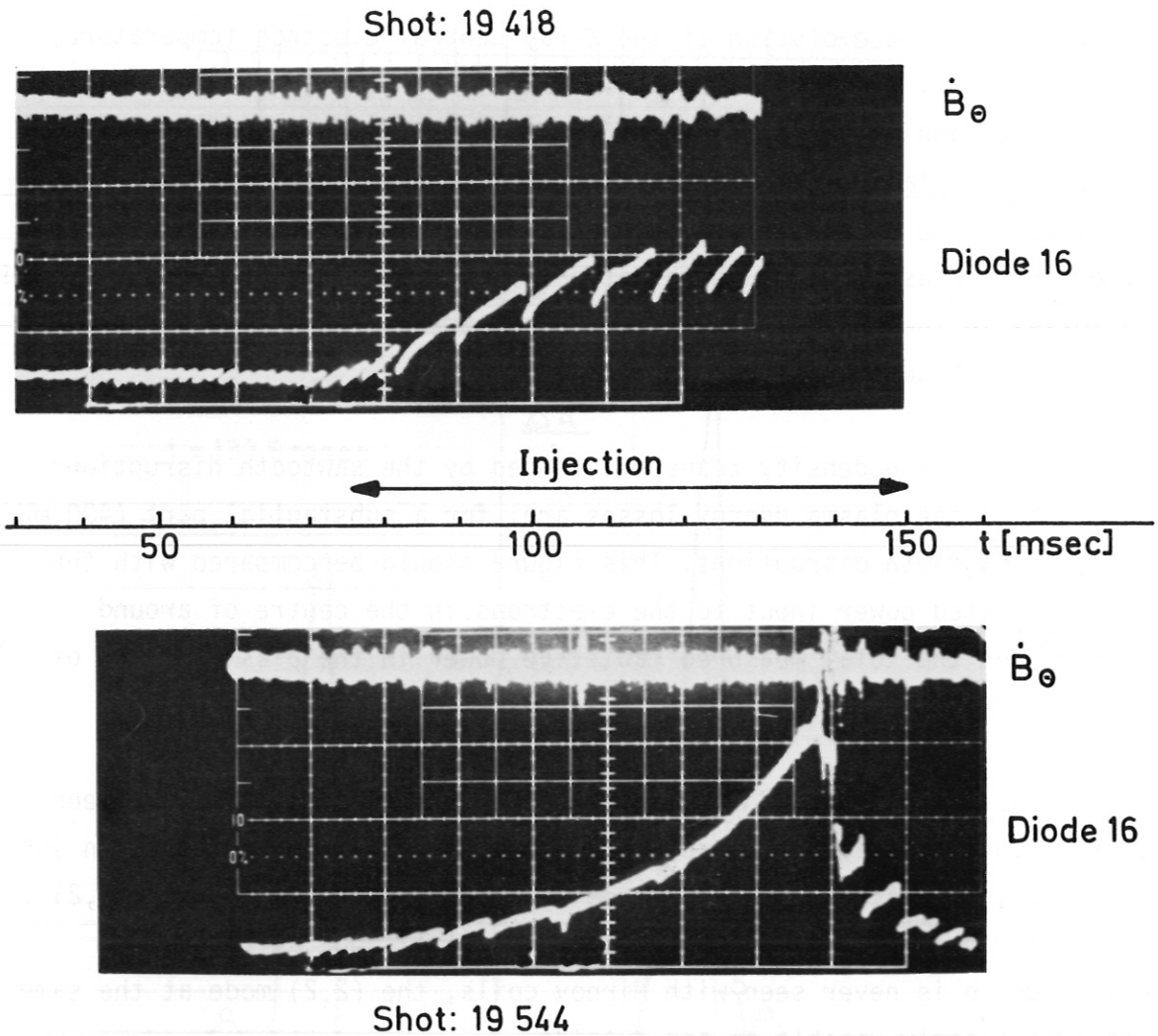

Fig. 7: Difference in sawtooth behaviour between pure helium discharges (Shot: 19418) and helium-deuterium mixture (Shot: 19544).

The lower part of the figure shows the time evolution for a helium-deuterium mixture. It can be seen that the sawtooth period also increases, but that is continues to increase. It can be seen on the right half of the figure that a sawtooth disruption caused by a (1,1) mode occurs a few msec before t = 140 msec and is later followed by a relatively large internal disruption caused by a (3,2) mode.

5.1. INTERNAL DISRUPTIONS AT THE q = 1.5 SURFACE

A typical time evolution of the USX fluxes for various radial positions is shown in Fig. 8 (shot 19544). At t = 135.5 msec the above-mentioned (1,1) caused sawtooth is hardly visible. At t = 138.5 msec the internal disruption caused by the (3,2) mode occurs. The precursor modes for the latter disruption are coupled (3,2) and (2,2) modes. The amplitude and phase radial profiles of these modes just before the disruption are given in the lower half of Fig. 9a for a similar shot. The structure of these modes has been determined by a set of Mirnov coils and the USX and SX diodes. Note that the amplitude of the modes is now much larger than for shot 19418 (Fig.6), especially the (2,2) mode.

5.2 SIMULATION OF THE (3.2) AND (2,2) PRECURSOR MODES

The left and upper part of Fig. 9a (shot 19561) shows the (3,2) and (2,2) modes during a 1 msec interval just before the internal disruption. These should be compared with the simulated signals /14/ on the right, which are produced by a fitted analytic X-ray emissivity distribution represented by the contour plot in the lower right half of the figure and also by the 3-dim. plot in figure 9b.

The simulated amplitude and phase radial profiles (broken lines) are given together with the measured profiles (solid lines) in fig. 9a.

The phase profiles show particularly good agreement between simulation and experiment. The discrepancies for the mode amplitudes are mainly due to the fact that in reality the modes are rapidly growing, especially towards the outside of the torus. Because of this the relative amplitude ($\Delta A^{\sim}/A$) rises

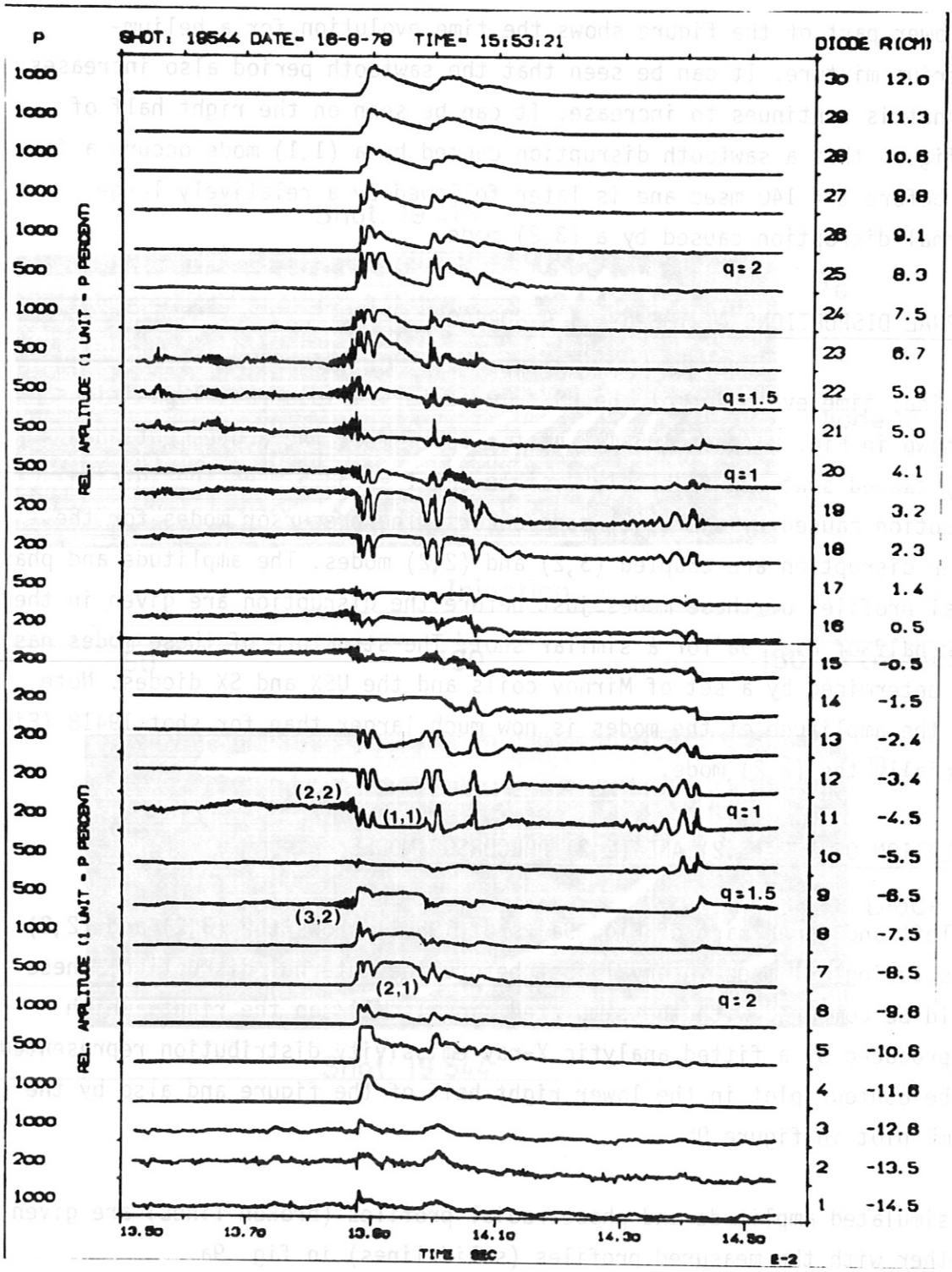

Fig. 8: Fast (3,2) + (2,2) modes (138.5 msec), internal disruption at q=1.5 (138.7 msec) and (1,1) + (2,1) modes (t_o=0.23, I_p=20 kA, 2 injectors, 2μBe, Shot: 19544).

well above two. This value is the maximum relative amplitude that can possibly exist for modes of constant amplitude and uniform rotation. Fig. 10 shows the Abel inverted X-ray intensity profiles just before and after an internal disruption at the q = 1.5 surface. This causes the profile to steepen near the q = 1 and q = 2 surfaces and to flatten at the q = 1.5 surface. (Note that the figure is on semi-log scale and that $\frac{dI}{dr} = I \frac{d\ln I}{dr}$). Assuming that the X-ray profile is a reflection of the electron temperature and therefore also the current density profile, the destabilization of the (1,1) and (2,1) modes can be expected.

5.3. THE AFTERMATH OF THE INTERNAL DISRUPTION AT THE q = 1.5 SURFACE

It has been observed that plasmas of the first type are more stable after an internal disruption at the q = 1 surface, although occasionally a (3,2) mode with constant amplitude may appear in between the sawtooth disruptions.

For the second type discharges it is usually found that the internal disruption at the q = 1.5 surface causes both the inside (1,1) and the outside (2,1) to become very unstable. This can be seen from the X-ray diode signals for shot 19544 in Fig. 8. The fast transition of the (3,2) and (2,2) modes structure during the disruption to a (1,1) and (2,1) modes structure is shown both on the X-ray and the Mirnov coil signals in Fig. 11.

The large (1,1) and (2,1) islands are correlated with a continuous plasma energy loss as is seen on the continuously decreasing central electron temperature (Fig. 12). The latter is measured with the filter method, which usually gives good agreement with other methods /5/.

The energy loss is also quite noticable on the plasma diamagnetism (total energy) and the plasma horizontal position. The latter change is also clearly visible on the USX-diodes: especially diodes Nos. 7 and 25 of Fig.8 (19544). (In order to compare both figures add 2.5 msec to the time scale of Fig. 8 (19544)). The plasma energy does not always decrease so smoothly. Changes in (1,1) and (2,1) mode behaviour may occur during sequential local disruptions, usually originating near the q = 1.5 surface. Some indication of this is also visible for shot 19544 on the outer USX diodes

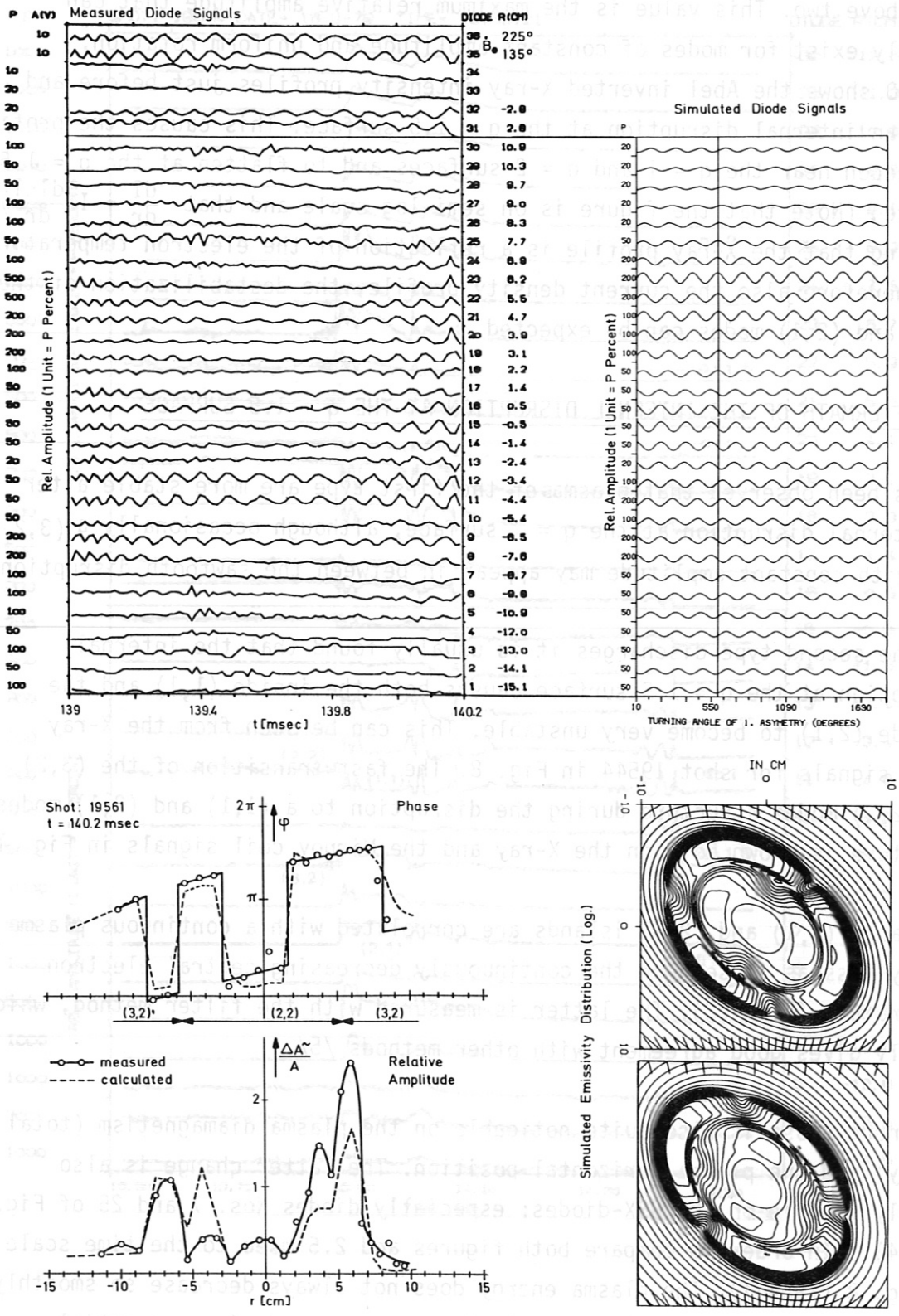

Fig. 9a: Coupling of (2,2) and (3,2) modes; comparison with simulation (Shot: 19561, t_0=0.23, I_p=20 kA, 2 injectors, 2μBe).

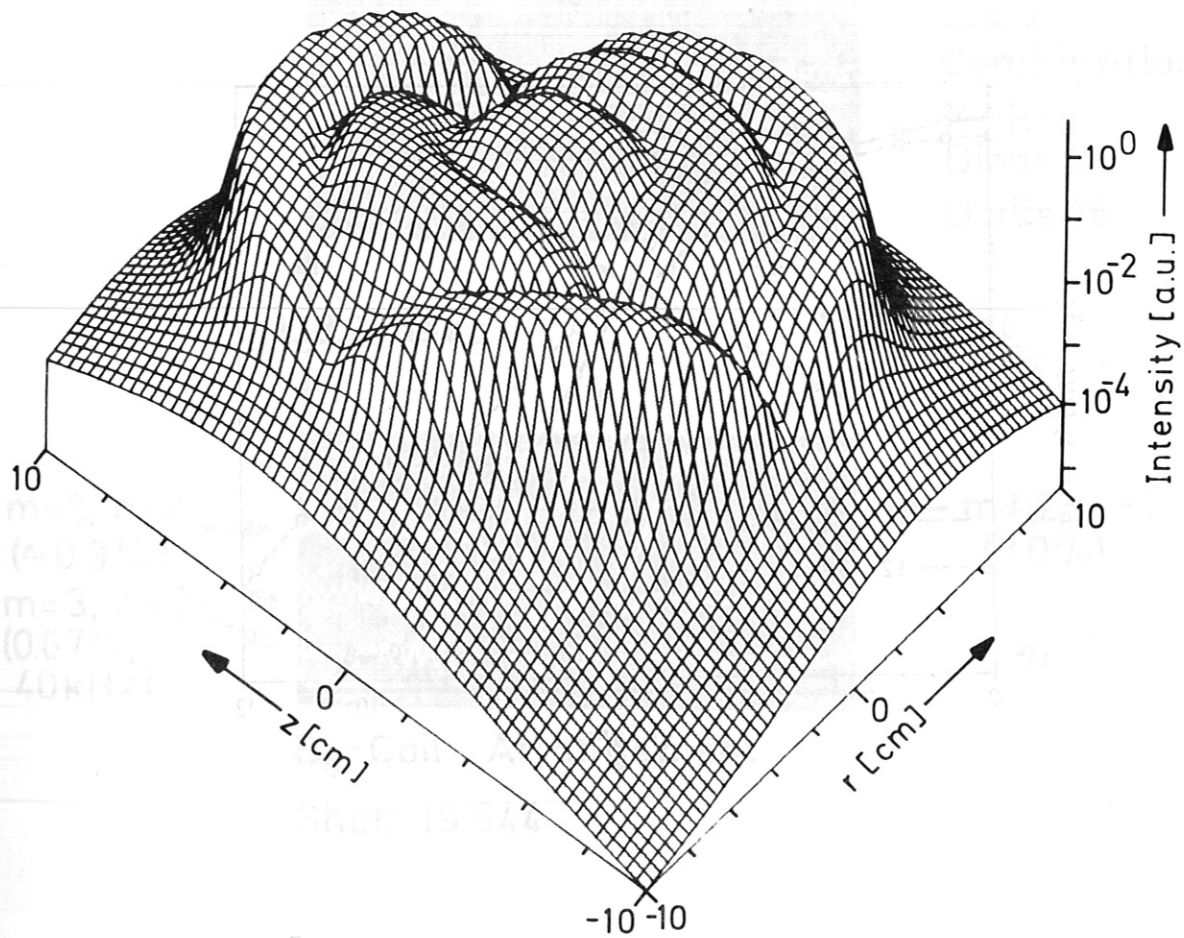

Fig. 9b: Simulated intensity distribution in the poloidal plane (Shot: 19561, coupling of (2,2) and (3,2) modes).

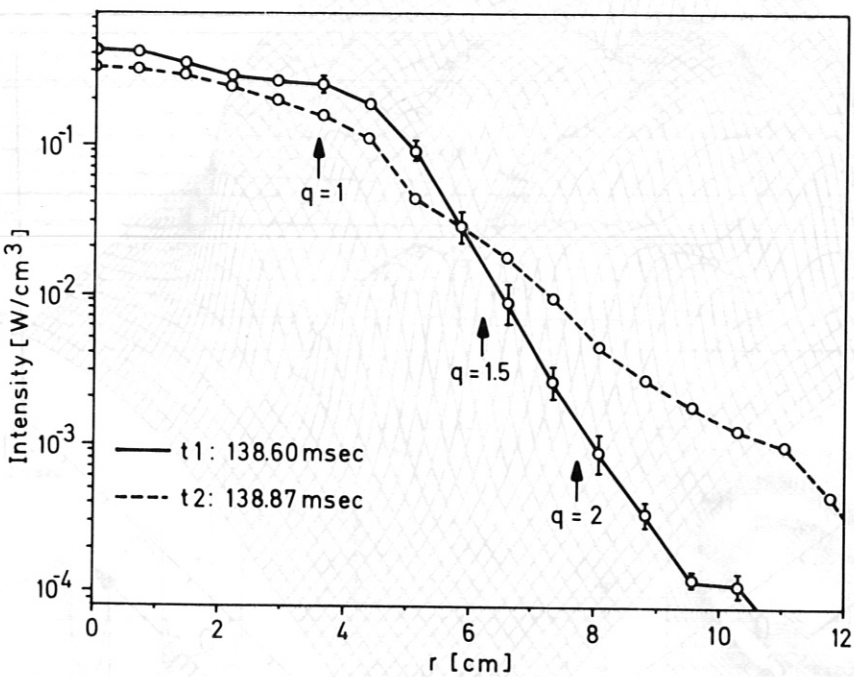

Fig. 10: USX intensity radial profiles before and after the (3,2) internal disruption
(Shot: 19544, t_o=0.23, I_p=20 kA, 2 injectors, 2μBe).

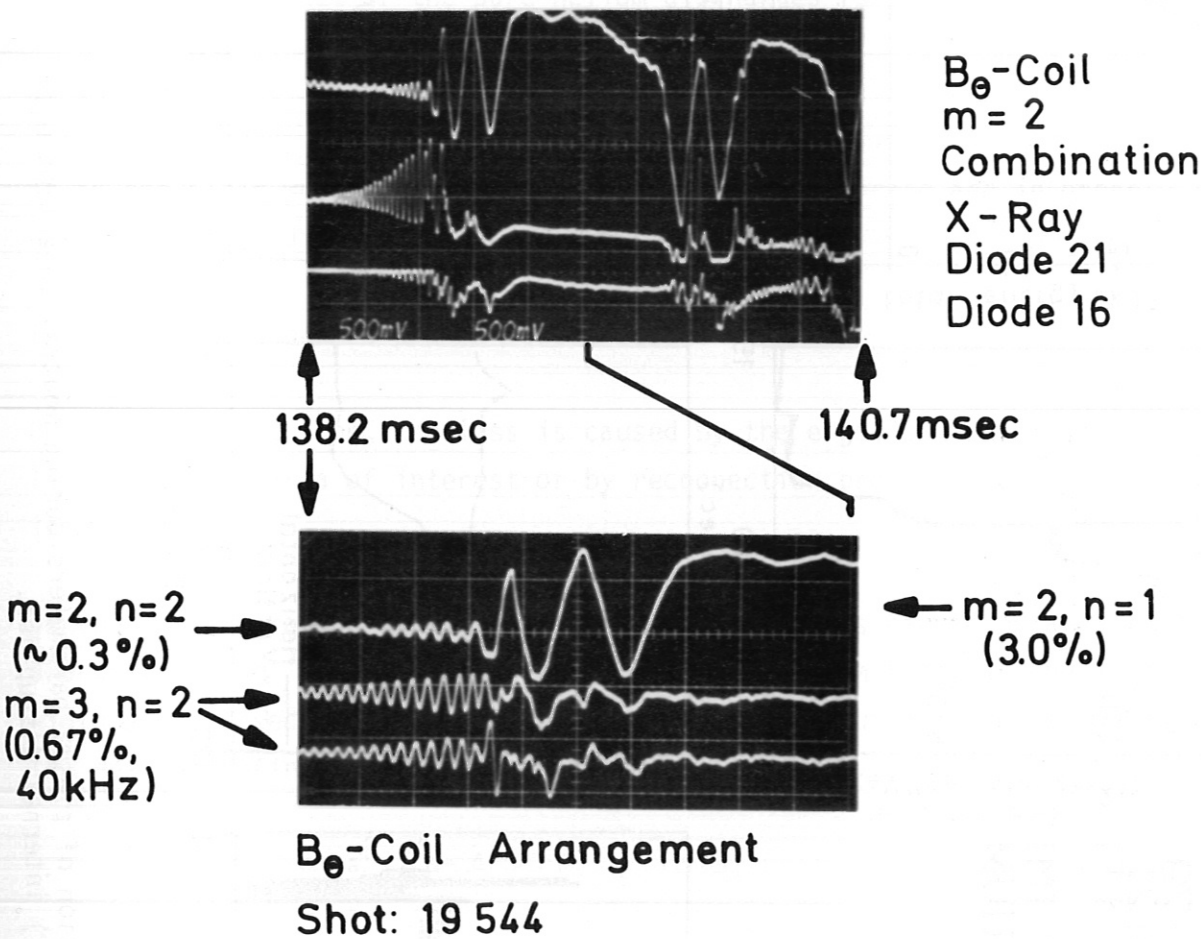

Fig. 11: Fast transition of (3,2) + (2,2) to (2,1) + (1,1) modes.

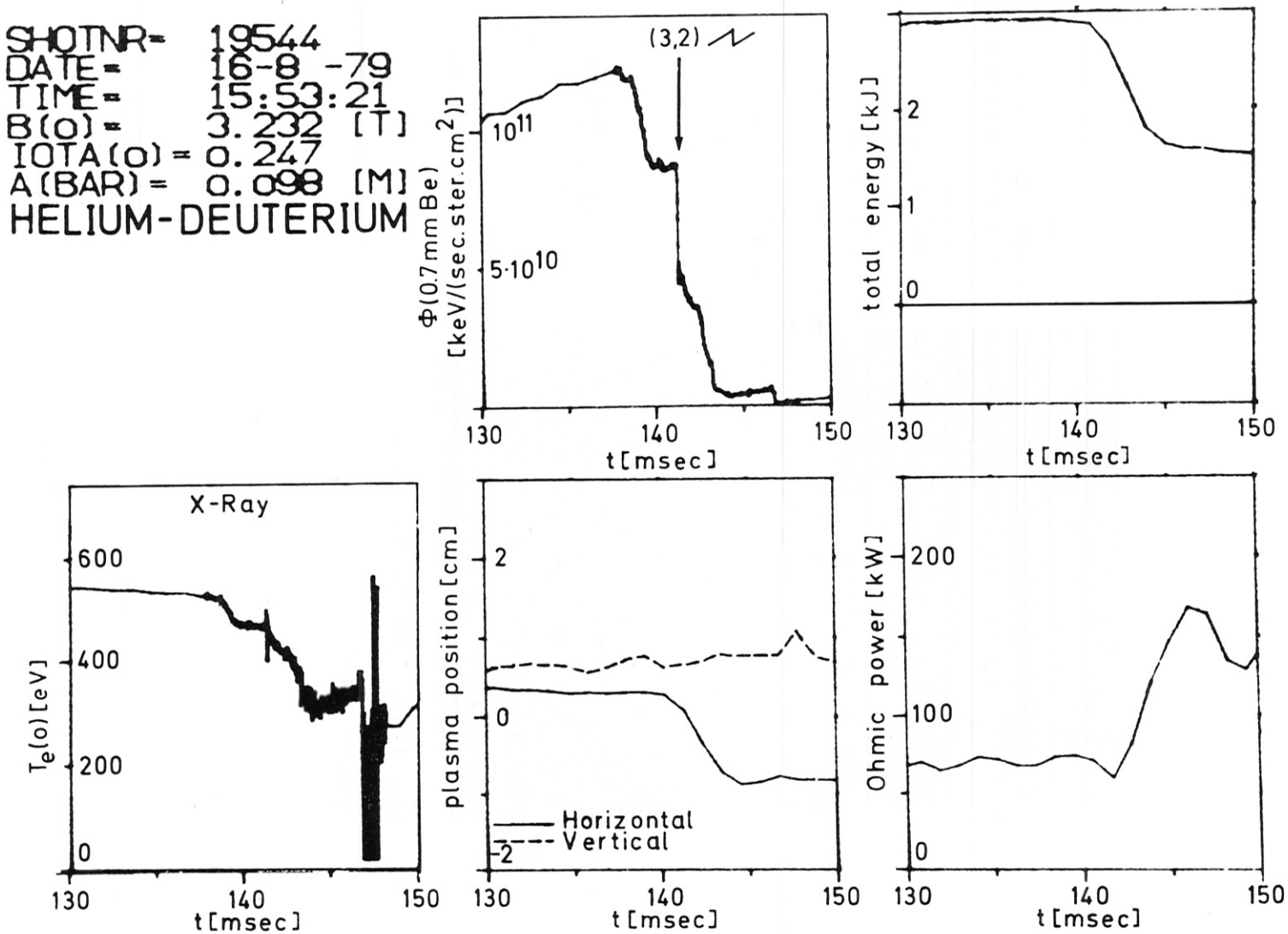

Fig. 12: Evolution of plasma parameters during Neutral Injection with a (3,2) internal disruption.

in Fig. 8. Further properties of the (1,1) and (2,1) modes will be discussed in the following sections.

The effects of the q = 1.5 disruption have died down at t = 141.5 msec (see Fig. 8) and transition to a normal q = 1 sawtooth discharge takes place. Apart from the lower T_e, radial profiles of the X-ray intensity of q = 1 and the position before and after the sawtooth disruption are very similar to that of the pure helium discharges (shots 19400 - 19435).

5.4. ENERGY LOSSES BY (1,1) AND (2,1) MODES

It is not clear why, in certain cases, the modes saturate and in other cases lead to a disruption.

In both cases enhanced plasma losses occur:

During the disruption, the loss is caused by the ergodisation of the field lines over the area of interest or by reconnection processes of the various islands.

During the saturation of the tearing mode the loss is caused by a virtual shortcircuiting of the perpendicular heat conduction K across the island width Δ/6/. Based on the increase of the gradients outside the islands, the energy confinement time τ_E can be calculated:

$$\tau_E \sim \frac{a^2}{\bar{K}} \cdot \frac{a-\Delta}{a} \qquad (1)$$

a = plasma radius or the region where gradients exists.

$\bar{K}$ = average heat conductivity

Assuming that the central temperature T_{eo} is correlated with its average value, one can derive that

$$\frac{dT_{eo}}{dt} \sim \frac{-\Delta}{a-\Delta} \cdot \frac{T_{eo}}{\tau_E} \qquad (2)$$

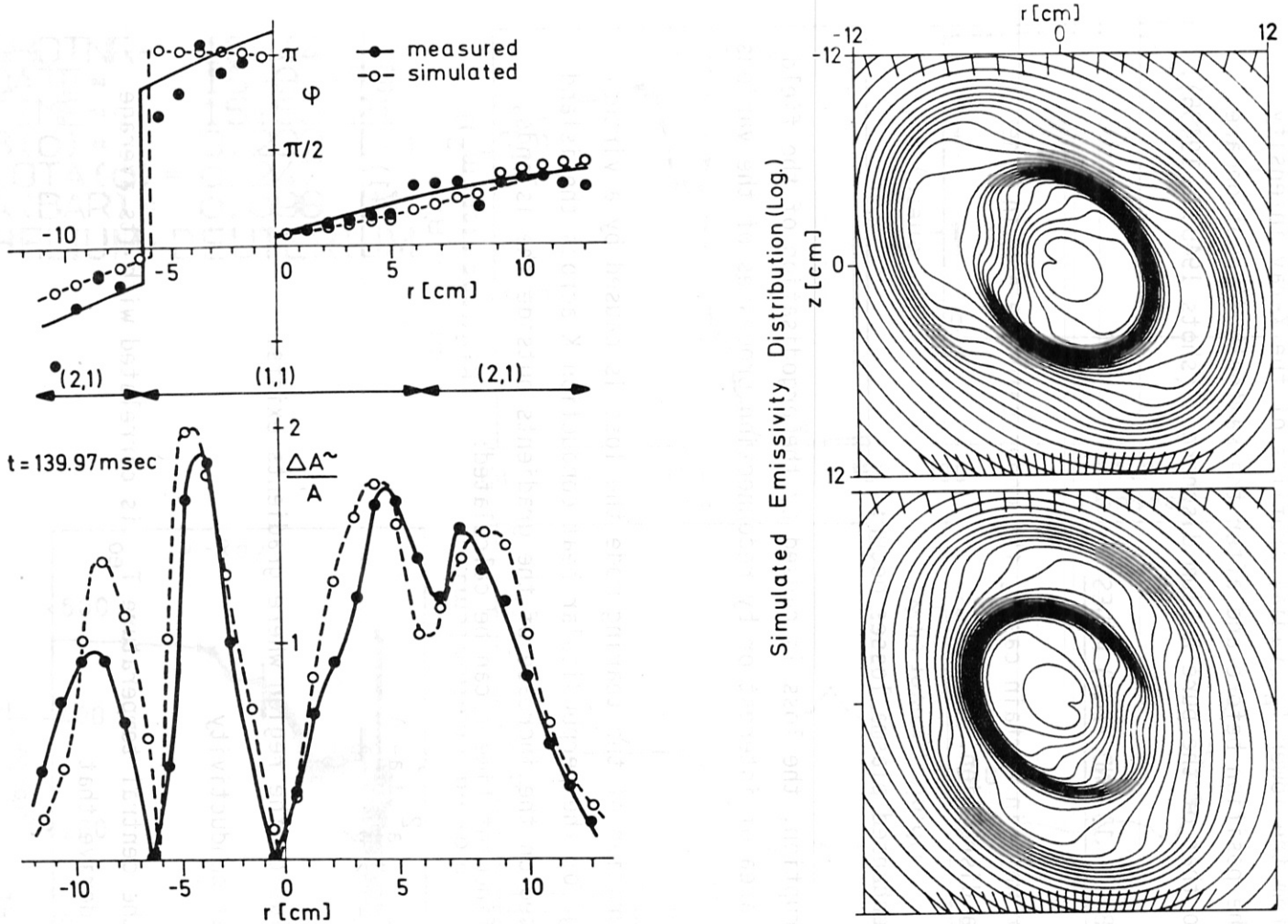

Fig. 13: Coupled (1,1) and (2,1) modes after (3,2)-disruption; comparison with simulation (left: phase and relative amplitude radial profiles; right: contour plots of simulated emissivity)
(Shot: 19544, t_0=0.23, I_p=20 kA, 2 injectors, 2μBe).

τ_E is the original energy confinement time, before the existence of the island(s). From the shape of the decrease of T_{eo} in Fig. 12, it can be found that $\Delta/a \sim 0.7$. Where Δ is the sum of the total shortcircuiting islands. If we assume the $\Delta\,(1,1) \sim r(q=1)$, this gives approximately 2.5 cm for the width of the (2,1) island. The plasma radius a is assumed to be ~ 10 cm. This value can be further reduced, because of the high radiation level at the plasma edge. (Radiative limiter /W VII-A Team, Prague/.) The value of the radius r(q=1) has been taken from the radius where the (1,1) mode has its maximum. This is shown in Fig. 13. Here the measured radial profiles of the relative amplitude and phase of the coupled (1,1) and (2,1) modes are given by solid lines in the left part of the figure. These have to be compared with the simulated curves (broken lines). The right-hand side of the figure shows the contour plots of the X-ray emission calculated by the simulation. The large size of the islands found in this way explains rather well the enhanced losses that have found experimentally.

5.5. MODE LOCKING

Another feature of the coupled (1,1) and (2,1) modes is that they may stop rotating over short periods.(In our example Fig.14 upper left part for 1 to 2 msec.) Correlated with the end of the locking interval is a change in the current density profile by a internal disruption. This can be derived by the change in the position of the q = 1 and q = 2 surfaces.

In all cases of so called mode locking the X-points of the separatrix of the (1,1) and (2,1) tearing modes are close to the upper-outer limiter segment /7/. This segment is the most severely subjected to the plasma - limiter interaction, because of the elliptical shape of the stellarator plasma and its horizontal position. Limiter mode locking has been regularly observed also in OH discharges with large (2,1) amplitudes and q(a) close to two.

Mode locking or reduction of the mode rotation has also been observed on TFR /8/ and ALCATOR A and C /9/. However, it seems in those experiments that the stagnation point is correlated with the O-point of the islands. This is the opposite of our interpretations.

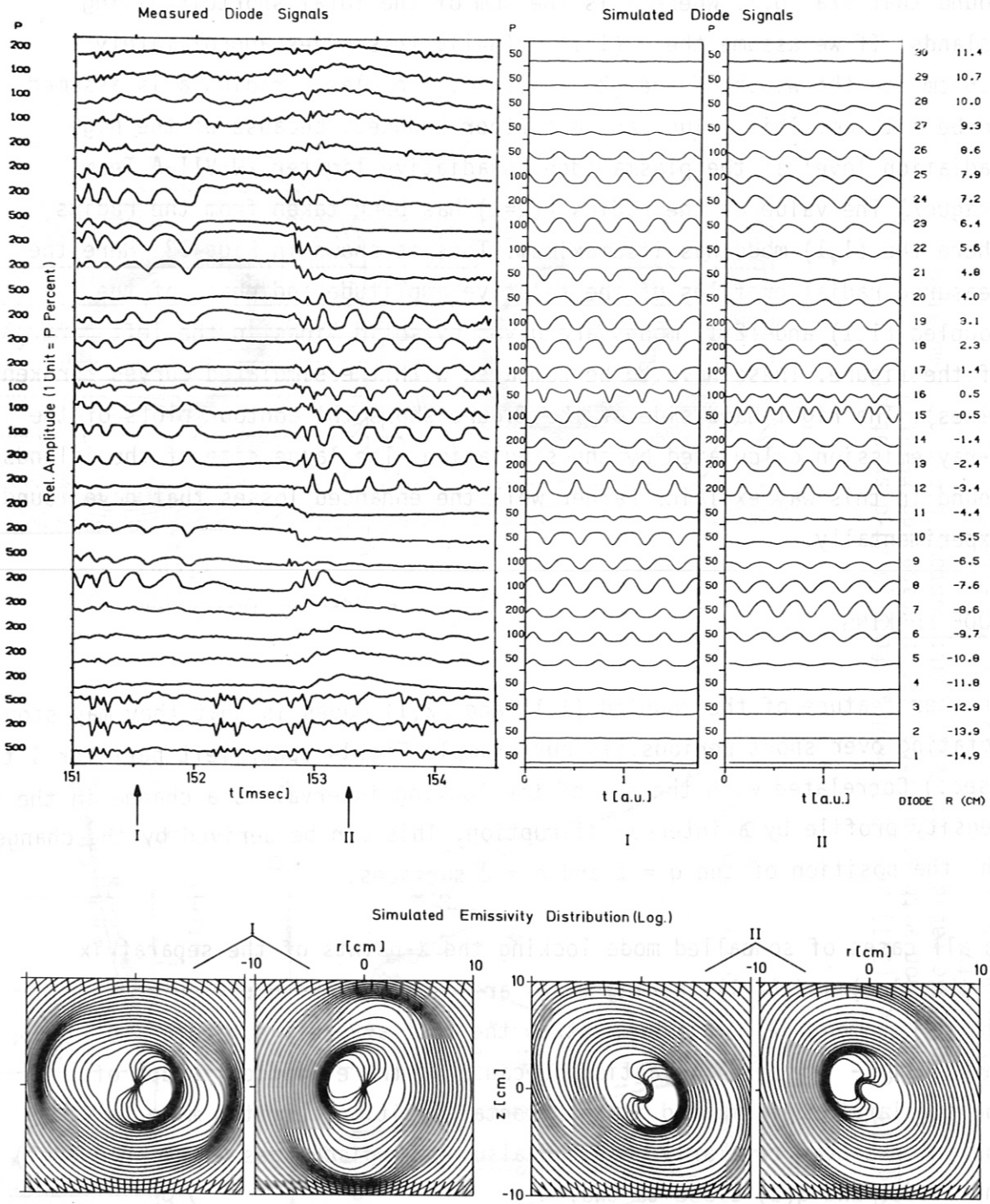

Fig. 14: Coupling of (1,1) and (2,1) modes; comparison with simulation two times (marked I, II)
(Shot: 18942, t_0=0.23, I_p=17 kA, 2 injectors, 2μBe).

Whether or not slackening of the rotation or locking occurs depends on the (2,1) island size and the distance between the q = 2 surface and the limiter. It is believed that both affect the drag of the limiter on the island and that further rotation is allowed when the island size is reduced or the distance to the limiter is increased. It is plausible that when the island tries to pass the cool limiter region it may shrink by partly quenching itself, therefore allowing further rotation. On the other hand it has also been observed (Fig. 8 shot 19544) that the rotation starts again during a local disruption. Here the disruption can force the current to flow more outside the q = 2 surface, thereby increasing the distance between that surface and the limiter.

5.6. SIMULATION OF THE (1,1) and (2,1) MODES

In addition to the measured X-ray signals simulated signals were calculated /14/ for the shot shown in Fig.14. In particular, the double frequency at t = 153 - 154 ms superimposed on the central USX signals can be well explained by the structure of the (1,1) island. The non-sinusoidal oscillations are partly caused by the poloidal extension of the islands and partly by a non-uniform rotation. The structures in the poloidal plane used for the simulation at two specific"times" marked I and II are shown in the figure. The emissivity is shown on logarithmic scale.

6. MAJOR DISRUPTIONS - LARGE (2,1) MODES

Without Neutral Beam Injection (NI) no major current disruptions occur if the external rotational transform ι_o is larger than 0.14.

The density limit for various values of the plasma current exceeds the Murakami limit significantly; by a factor of 3 to 4. At external rotational transforms of $\iota_o > 0.14$ the density limit no longer depends on disruptions /12/. The appearance of major disruptions is clearly linked with the presence of strong (2,1) modes. The increase in the (2,1) mode activity with increasing density is correlated with the increased radiation losses at the

plasma edge. This behaviour could be explained by the modification of the current density radial profile due to the edge cooling /13/. It has also been observed that a general decrease of the m = 2 mode activity with increasing ι_0 occurs /7,11/. This effect together with the additional plasma equilibrium provided by the helical stellarator field are stabilizing the plasma against major current disruptions /12/.

An important aspect of these disruptions is that several modes ((2,1) + (1,1)) play a role in the process. In particular, the edge cooling forces the q = 1 surface to move outwards, diminishing the distance between the rational q-surfaces /12/.

Without Neutral Beam Injection the m = 2 mode and the major current disruptions disappear for high ι_0 ($\iota_0 \geq 0.14$ to 0.17). This could be understood by the fact that the rational q = 2 surface moves outwards with increasing ι_0 towards regions with less and less current density. With Neutral Beam Injection large (2,1) modes appear under certain conditions also at high values of $\iota_0 \gtrsim 0.20$. Occasionally major disruptions occur then.

Qualitatively, the destabilization of the (2,1) mode with NI can be understood as being caused by the enhanced edge heating which increases the current density near the q = 2 surface. This effect is amplified by the occurrence of internal disruptions at q = 1.5.

New aspects of the major disruptions during NI are that most disruptions observed occurred usually with only one predominant precursor mode present and also at lower plasma currents. The precursor mode of a (2,1) structure was occasionally accompanied by a much smaller phase coupled (1,1) mode.

In these discharges, however, other large modes were observed a while before the (2,1) caused major disruption. These other modes cooled the plasma centre. Enhanced cooling of the plasma centre or heating of the

plasma edge forces the q = 1 and q = 2 surfaces radially inward by changing the current density profile. The q = 1 surface may even disappear, in which case a large (2,1) mode can grow in a region with reduced shear. Extensive (2,1) modes have indeed been observed as will be shown in the following examples.

6.1. GENERAL DESCRIPTION OF THE TIME EVOLUTION BEFORE A MAJOR CURRENT DISRUPTION

The examples show the time evolution of the USX and Mirnov coils signals before and during the (2,1) disruption. The plasma parameters for these discharges are close to those discussed in Chapter 5.1: t_o = 0.19, I_p = 17 - 20 kA, He and D mixture, 2 injectors, and average plasma beta $\sim 10^{-3}$. Again the characteristic feature is the relatively long time interval (~20 msec) with only a very small mode activity. But in this case, a (3,2) mode is growing very slowly ($\gamma \sim$ 33 sec^{-1}) in contrast with the rapidly growing (3,2) mode discussed in Chapter 5.1. It is likely that in most cases the (3,2) mode is coupled with a (2,2) mode, although this has not been extensively analysed. Usually, after a localized internal disruption at the q = 1.5 surface, large coupled (1,1) and (2,1) modes appear which decay progressively, leaving a quiescent plasma for a period of 1 msec. Apparently, during this period there is a reorganization of the current density radial profile because a large growing (2,1) mode appears afterwards, coupled with a (1,1) mode of varying amplitude. Sometimes, the (1,1) is hardly visible at all, and a single (2,1) mode is present. Usually, these large single (2,1) modes lead to a current disruption.

6.2. FIRST EXAMPLE

Fig. 15 shows the time evolution of the USX diodes and some of the Mirnov coils, from a few milliseconds before the supposed q = 1.5 disruption until after the main q = 2 disruption for shot 18921. It is difficult to determine whether the localized disruption occurs at the q = 1.5 surface, because the precursor mode is not clearly visible on the USX diodes, since too few sampling points over the long time that the mode is growing are taken. However, the inversion radius of the disruption is close to 4.7 cm,

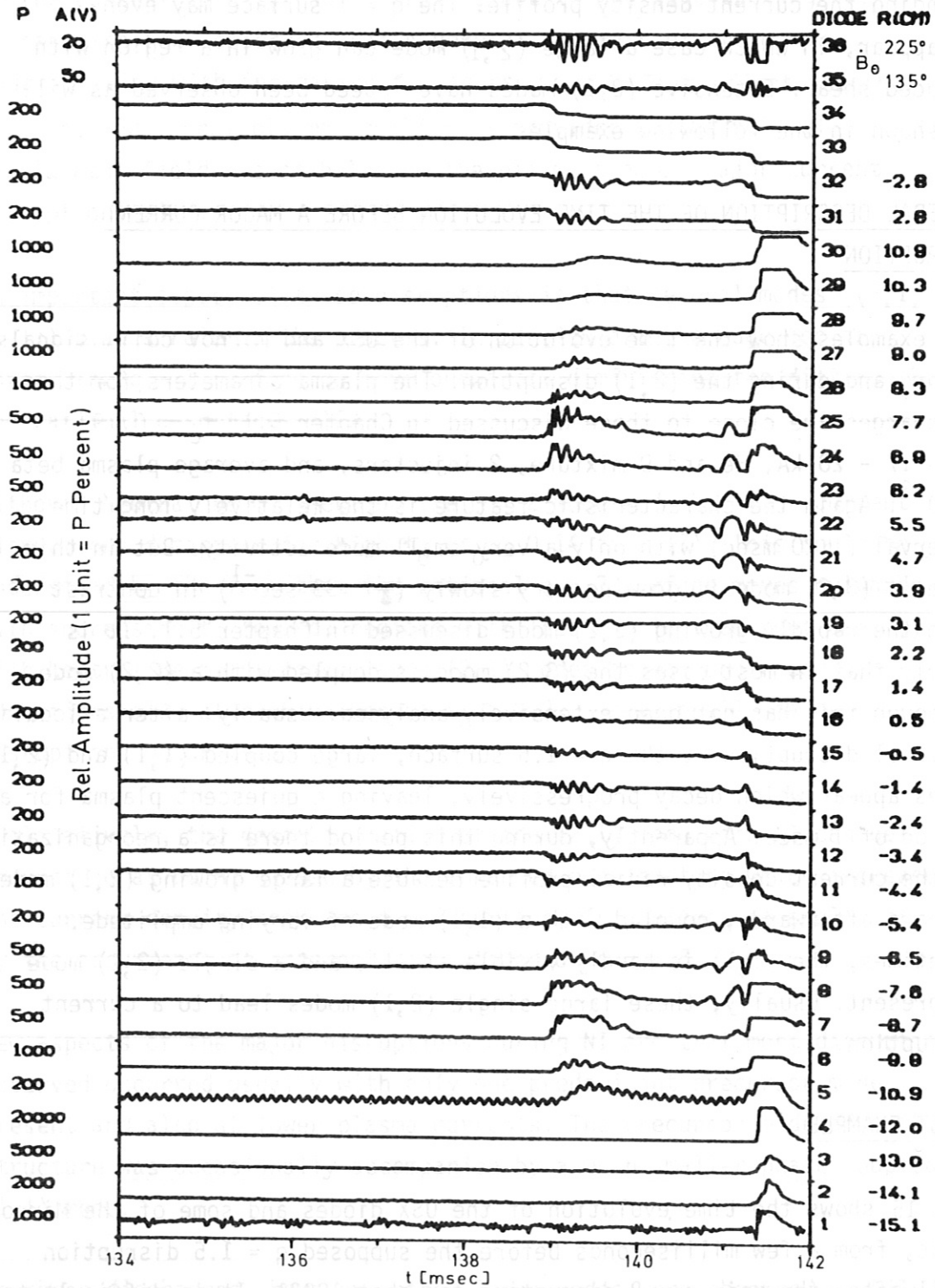

Fig. 15: Diode signals preceding major disruption
(Shot: 18921, t_0=0.19, I_p=20 kA, 2 injectors, 2μBe).

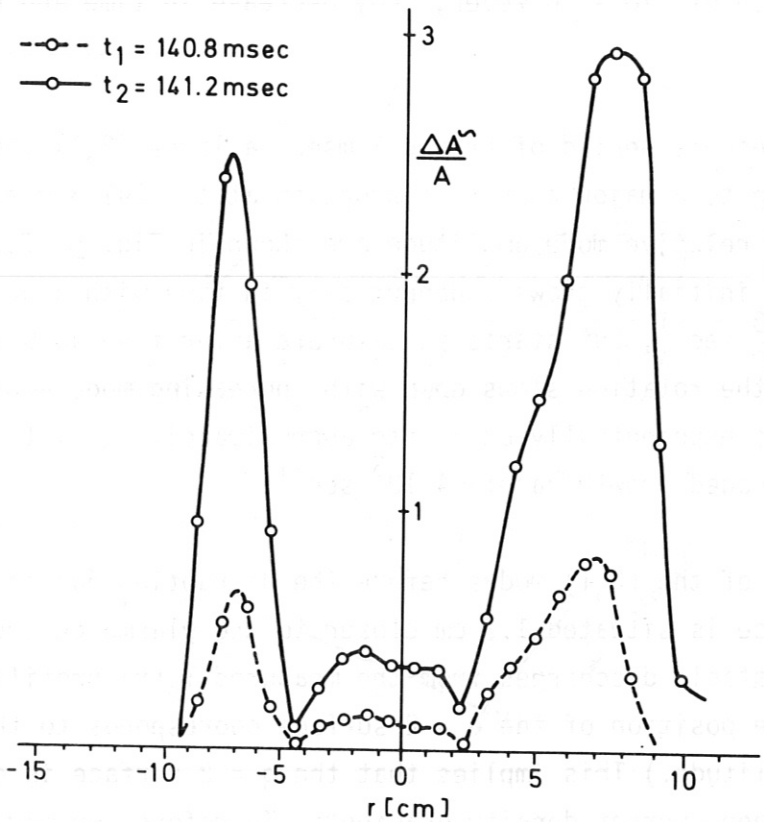

Fig. 16: Radial profiles of large growing (2,1) mode at two subsequent times t_1, t_2 just before major disruption (Shot: 18921, t_0=0.19, I_p=20 kA, 2 injectors, 2μBe).

whereas the q = 1 and q = 2 surfaces are situated at 3 and 7 cm. This has been determined from the maxima of the (1,1) and (2,1) modes that appear during and after the disruption.

The situation therefore looks very similar to the discharges discussed in Chapter 5.1 (shot 19544), although here the external t_0 was larger, possibly being the reason why no major current disruption occurred later on. (Remember that the q = 2 surface is closer to the outside for larger values of t_0.) Also there the (3,2) mode started to develop with a "normal" faster growth rate. The large coupled (1,1) and (2,1) modes have a modulation of 70 %. However, they decrease in time and disappear completely.

Following a quiescent period of around 1 msec, a large (2,1) mode starts to grow, leading to a major current disruption at t = 141.3 msec. Radial profiles of the relative mode amplitude are shown in Fig. 16 for two times. The mode initially grows exponentially in time with a growth rate $\gamma \sim 5.6 \pm 0.6\ 10^3\ \text{sec}^{-1}$, but starts to saturate after t = 140.9 sec. Typically also the rotation slows down with increasing mode amplitude. This also occurs exponentially at a rate approximately equal to that of the time averaged growth rate: $\sim 4 \cdot 10^3\ \text{sec}^{-1}$.

Another feature of the (2,1) modes before the disruption during NI is that the q = 2 surface is situated 1.7 cm closer to the plasma centre than calculated for stable discharges from the measured $T_e(r)$ profile. (It is assumed that the position of the q = 2 surface cooresponds to the maximum of the mode amplitude.) This implies that the q = 2 surface is closer to regions with steep current density gradients. Therefore, we may expect the (2,1) to be more unstable. This may explain the occurence of major current disruptions at lower plasma currents, as is shown in the third example. Because a lower plasma current implies a more inward located q = 2 surface.

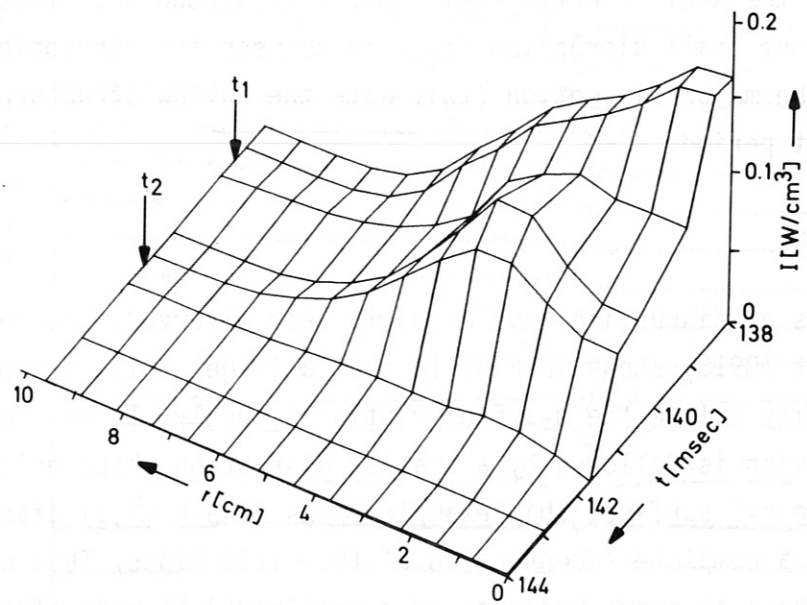

Fig. 17: Evolution of the radial USX intensity profiles during subsequent disruption: at q=1.5 at t=t_1 and a major disruption at q=2 at t_2
(Shot: 18921, t_o=0.19, I_p=20 kA, 2 injectors, 2μBe).

6.3. HOLLOW EMISSION PROFILES AND THE q=1 SURFACE

Shrinkage and disappearance of the q=1 surface seems to be correlated to larger extended (2,1) islands. The shrinkage of q=1 may be supported by the fact that inbetween the smaller and larger disruption, during the quiescent period, hollow USX emission profiles are observed. The USX emission is mainly due to (line) radiation between 600 - 1000 eV, probably the K-lines of O^{7+} (oxygen being the most abundant impurity) so that a hollow profile may indicate a lower abundance in the centre of O^{7+} as compared to the fully ionized O^{8+}. This is some evidence for the assumed disappearance of the q=1 surface, which, when present leads to a flattening of the profiles in the central region. Fig. 17 gives the time evolution of the Abel inverted radial profiles of the USX emission through 2μBe before the small disruption (t_1), in between the disruptions, and just after the major disruption (t_2). Note the hollow structure during the quiescent period.

6.4. SECOND EXAMPLE

Various types of disruption have actually been observed. The second example (shot 18918) shows in Fig. 18 that a large (2,1) disruption may not necessarily follow the q=1.5 disruption directly. In this case, the q=1.5 disruption is followed by a smaller disruption which originates mainly at the q=2 surface. This example shows a weak (2,1) disruption, even without a complete reconnection of the field lines. This can be deduced from the continuous presence of a smaller (2,1) mode after the disruption. A large scale disruption has possibly been prevented by the presence of the q=1 surface. This presence can readily be deduced from the clearly visible (1,1) mode before and after the local disruption. (Up to 200 % modulation after the disruption). After the evanescence of the (1,1) mode, a quiescent period follows. During this period the q=1 surface probably shrinks, since a (2,1) mode starts to grow, which leads to a major disruption. Fig. 19 shows the time evolution of Abel inverted USX radial profiles. Here also the hollow structure of the emissivity during the quiescent period is visible.

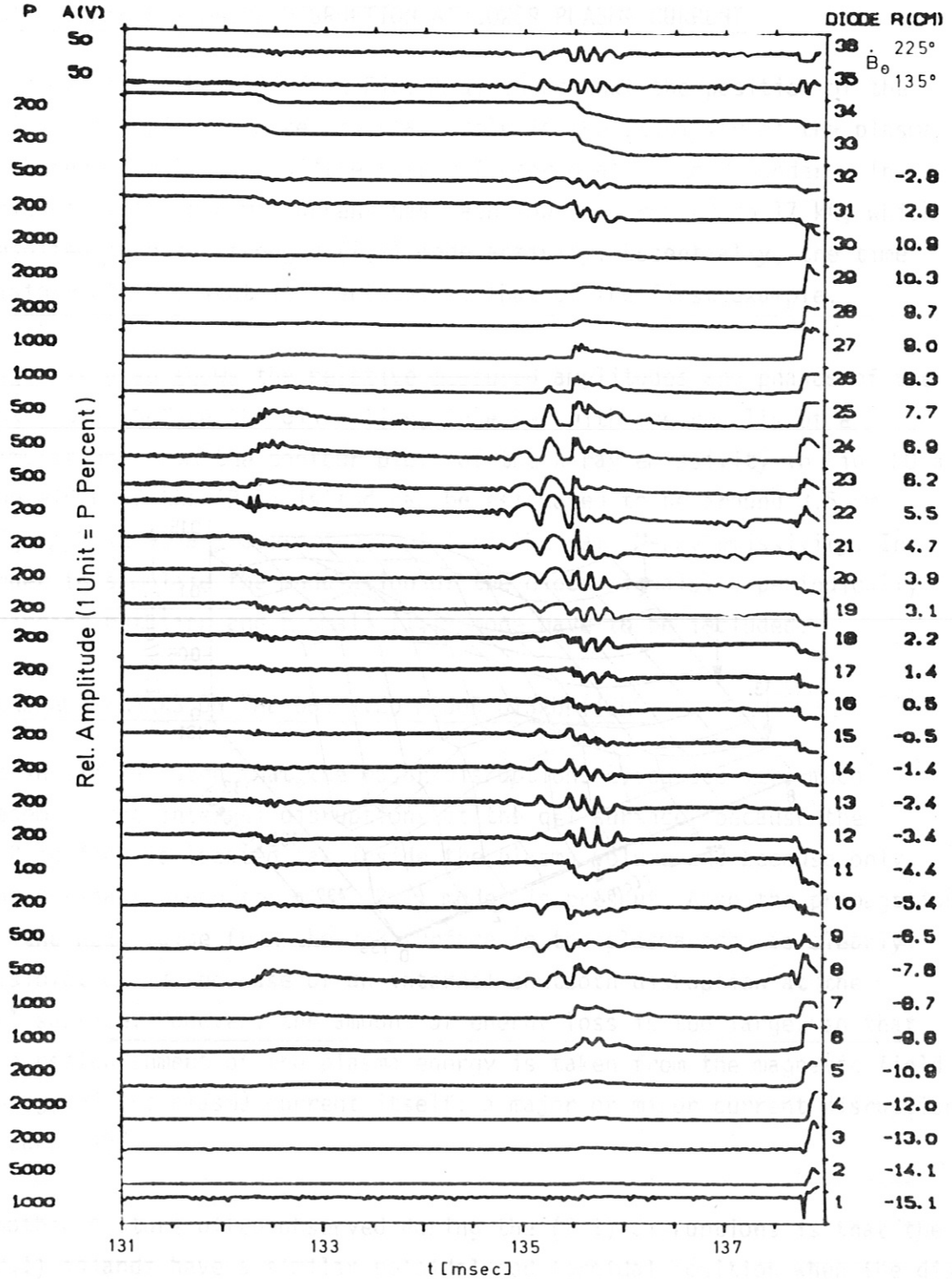

Fig. 18: Diode signals preceding major disruption
(Shot: 18918, t_0=0.19, I_p=20 kA, 2 injectors, 2μBe).

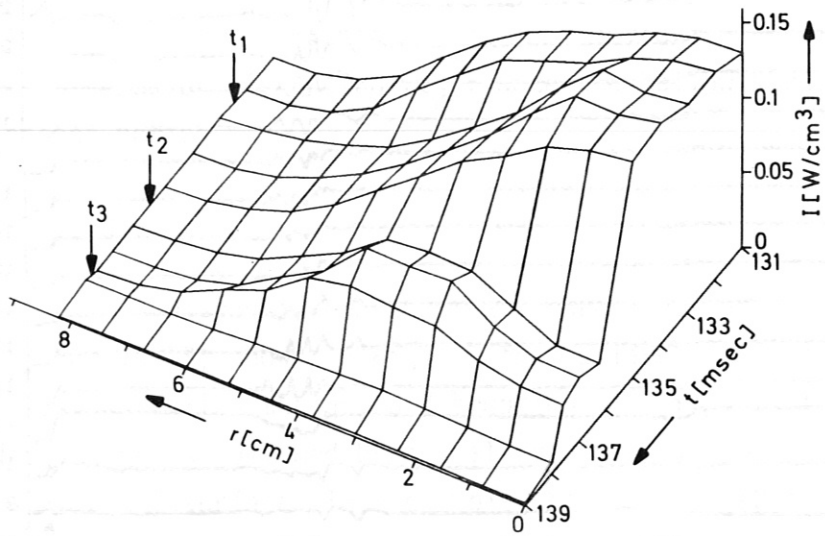

Fig. 19: Evolution of the radial USX intensity profiles during subsequent disruption: at q=1.5 at t=t_1, at q=1 or 2 at t_2 and a major disruption at q=2 at t_3
(Shot: 18918, t_0=0.19, I_p=20 kA, 2 injectors, 2μBe)

6.5. THIRD EXAMPLE - MAJOR DISRUPTION AT LOWER PLASMA CURRENT

This example (shot 18886 in Fig. 20a) shows that the position of the q=2 surface plays a more important role in the stability of the plasma than the actual value of the safety factor q(a) at the boundary. In this case, the plasma current has been lowered from 20 to 17 kA, which resulted in even stronger (2,1) mode activity. Essentially, the time history of this shot is identical to that of the first example.

Fig. 20a also shows the relative measured amplitudes and phases of the USX diodes before the disruption, together with the results of a simulation. From the contour plots of the X-ray emissivity in Fig. 20 a the width of the (2,1) island can be estimated to be around 3.5 cm. Fig. 20b shows a 3 dimensional plot of the same X-ray emissivity. In order to simulate the modulation of the diode signals, a periodically changing rotation and a small (1,1) mode have to be included.

6.6. GENERAL REMARKS ON THE OBSERVED MAJOR DISRUPTIONS

It should be noted that the major disruptions discussed very much resemble the internal disruptions at the q=1 surface, because the q=2 surface is located far inside the plasma volume and because only one dominant precursor, the (2,1) mode, is present. Also the propagation of the heat pulse from the q=2 surface to the plasma edge is clearly visible, as in the case of an internal sawtooth disruption at the q=1 surface. However, the amount of energy loss is too large, so that the replenishment of the plasma energy is taken from the magnetic field energy of the plasma current itself: a major or minor current disruption occurs /12/.

Another feature often observed during the (2,1) disruptions is that the (2,1) islands have a similar poloidal and toroidal position when the disruption takes place. This is an indication of the interaction between the (2,1) island and some obstacle at the plasma edge. As in the case of the mode locking discussed in Chapter 5.5 the X-point of the separatrix of the (2,1) mode seems to be close to the outer and upper limiter. However, in this case, although a continuously slowing down of the mode rotation is observed, no strong locking with the limiter is detectable, at most a periodically changing rotation is observed.

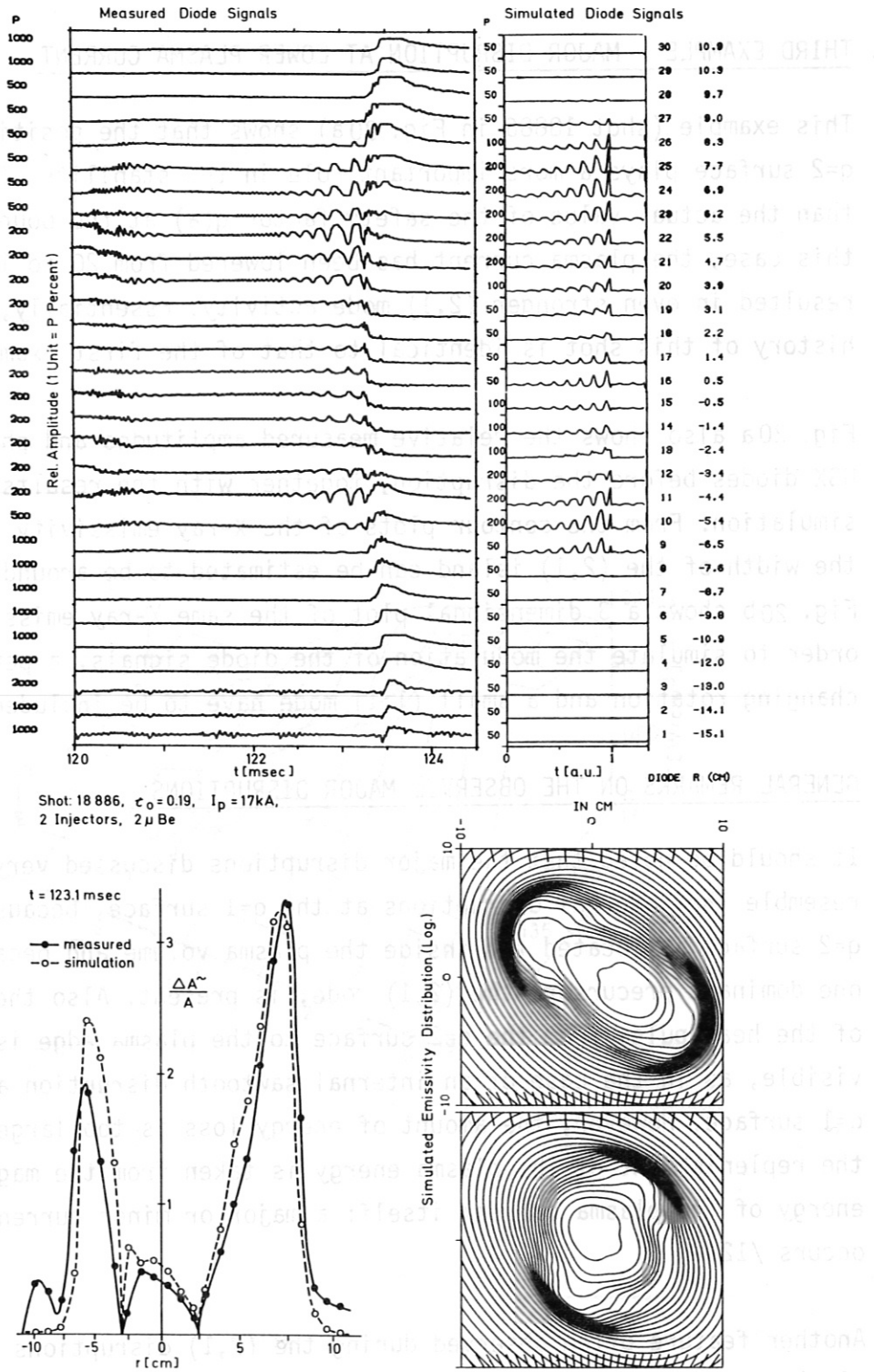

Fig. 20a: Large (2,1) mode (with a smaller (1,1) component) causing a major disruption; comparison with simulation

upper left: measured diode signals

upper right: simulated diode signals

lower left: radial profile of relative amplitudes

lower right: simulated emissivity distribution

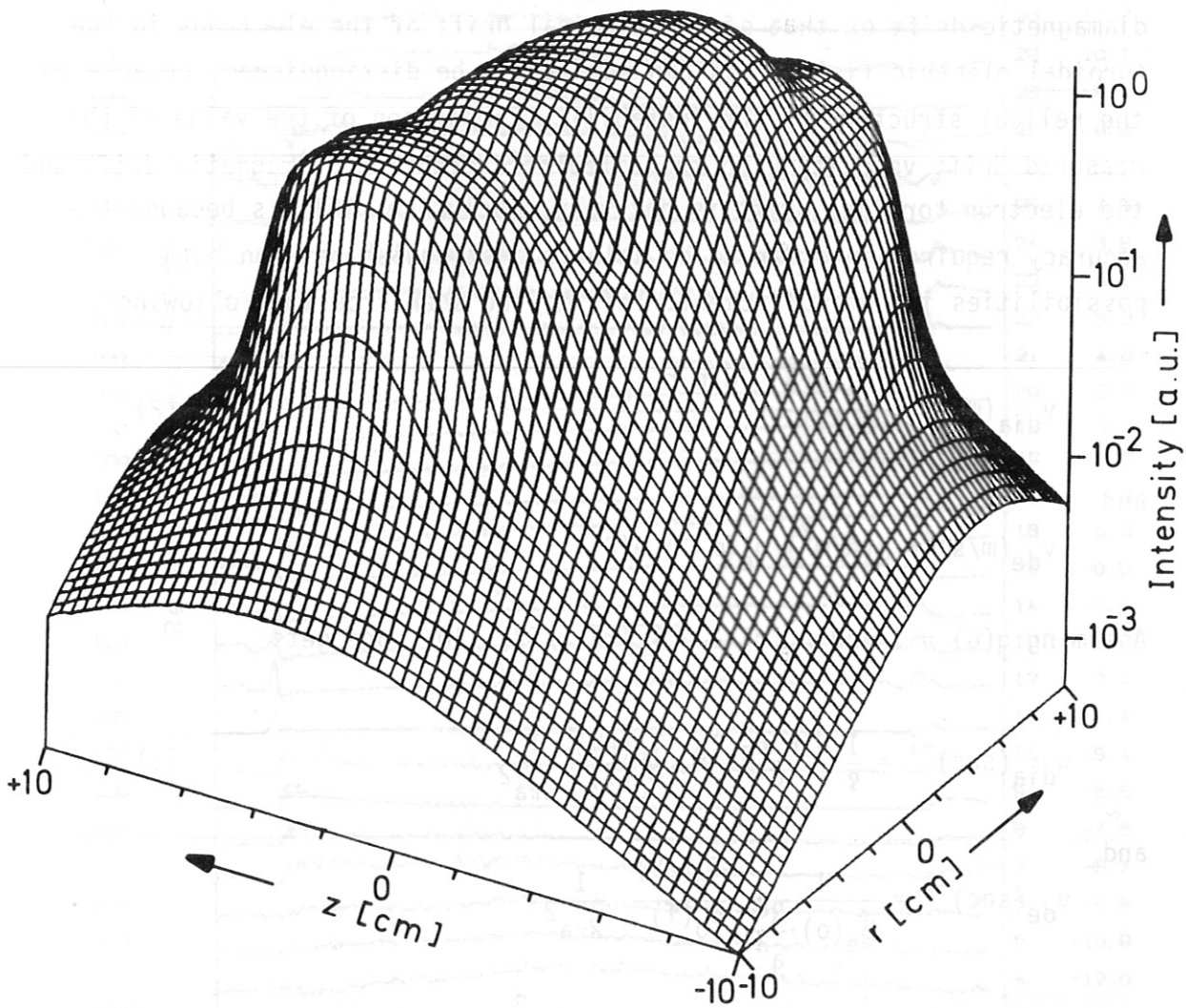

Fig.20b: Fitted intensity distribution in the poloidal plane which is used in the simulation for shot 18886 just before major disruption.

7. THE DIRECTION OF ROTATION OF THE TEARING MODES

The direction of rotation of the tearing modes does not change during Neutral Beam Injection, probably because of the nearly perpendicular injection. This is in contrast with other experiments, which have tangential injection, such as PLT or ISX.

The rotation is either in the direction of the poloidal electron diamagnetic drift or that of the toroidal drift of the electrons in the toroidal electric field. This can not easily be distinguished, because of the helical structure of the instability.Comparison of the value of the measured drift velocity with the calculated electron diamagnetic drift and the electron toroidal drift is not very conclusive. This is because the accuracy required in order to be able to distinguish between both possibilities is not sufficient. This may be seen from the following:

$$v_{dia}(m/s) = \frac{T_e(eV)}{B_o(T)} \cdot \frac{d\ln n_e T_e}{dr} \qquad (2)$$

and

$$v_{de}(m/s) = j(A/m^2)/n_e(m^{-3})\ e(C).$$

Assuming $q(o) = 1$ and $n_e(r) \sim \sqrt{T_e(r)}$ /5/, /10/, one gets

$$\nu_{dia}(sec)^{-1} = \frac{1}{\varrho} \frac{d\ln n_e T_e}{d\varrho} \cdot \frac{T_e(eV)}{B_o(T)} \frac{1}{2\pi a^2} \qquad (3)$$

and

$$\nu_{de}(sec)^{-1} = \frac{4}{\beta_e(o) \cdot \frac{R^2}{a^2}} \frac{T_e(eV)}{B_o(T)} \frac{1}{2\pi a^2}$$

with $\varrho = r/a$ and $\beta_e(o) = n_e(o) \cdot T_e(o) / B_o^2 / 2\mu$.

This yields the following relation

$$\frac{\nu_{dia}}{\nu_{de}} = \frac{\beta_e(o) \cdot R^2/a^2}{4\varrho} \cdot \frac{d\ln n_e T_e}{d\varrho} \qquad (4)$$

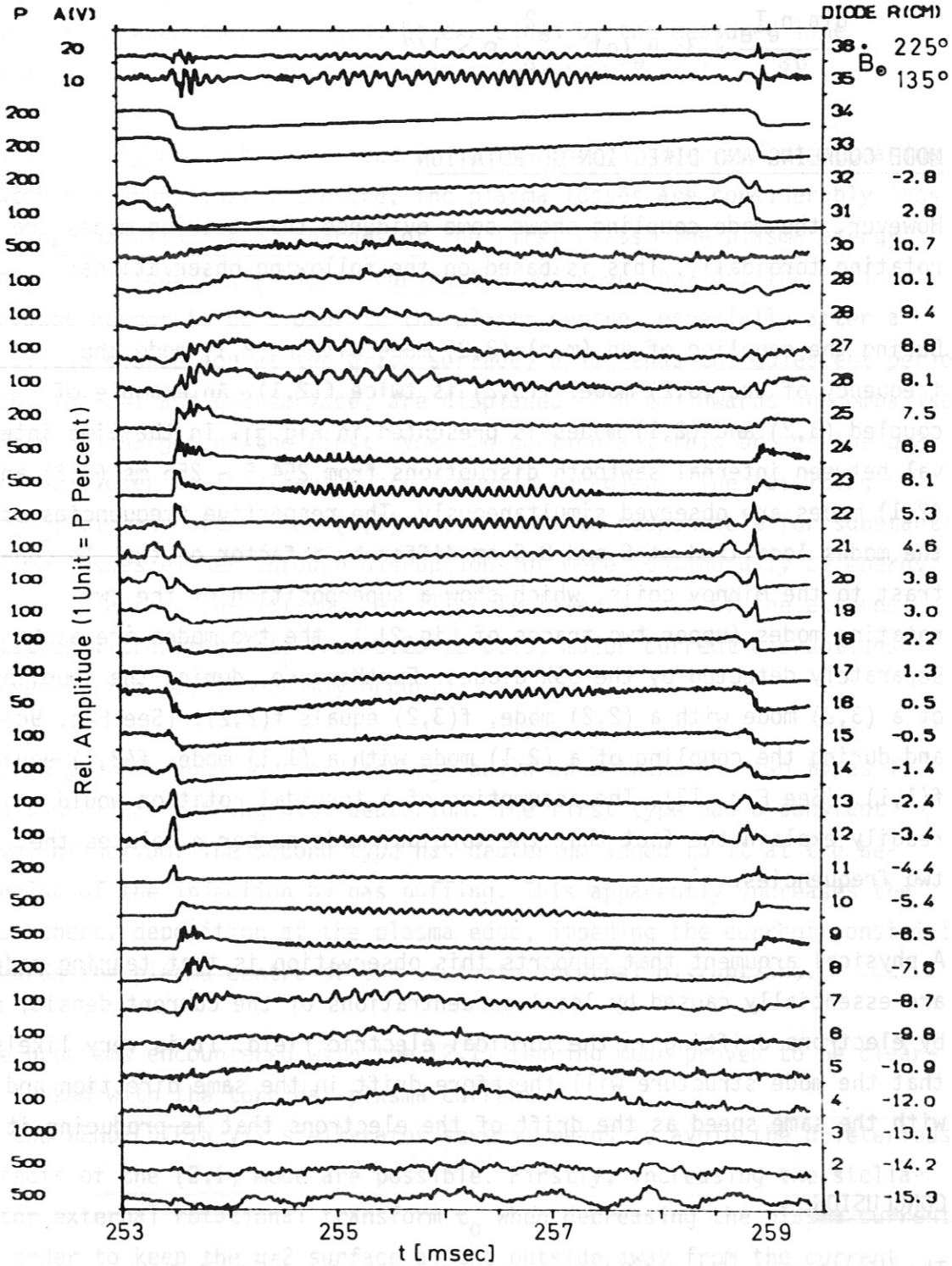

Fig. 21: Transition of coupled (3,2) + (2,1) modes to coupled (1,1) + (2,1) modes (t_0=0.17, I_p=25 kA, 1 injector, 2μBe, Shot: 18642).

In practice this ratio is of the order of unity:

$$\frac{d \ln n_e T_e}{d\varrho} \approx 3; \; \beta_e(o) \approx \frac{a^2}{R^2}; \; \varrho \gtrsim 1/2 \; .$$

7.1. MODE COUPLING AND DIRECTION OF ROTATION

However, the mode coupling shows some evidence that tearing modes are rotating toroidally. This is based on the following observations:

During the coupling of an (m,n)=(3,2) mode with a (2,1) mode the frequency of the (3,2) mode: f(3,2) is twice f(2,1). An example of coupled (3,2) and (2,1) modes is presented in Fig. 21. In the time interval between internal sawtooth disruptions from 254.5 - 256 ms (3,2) and (2,1) modes are observed simultaneously. The respective frequencies of the modes localized at 6 and 8.5 cm differ by a factor of two. In contrast to the Mirnov coils, which show a superposition of the two rotating modes (upper two traces of Fig. 21), the two modes are each separately detected by the USX diodes. Furthermore, during the coupling of a (3,2) mode with a (2,2) mode, f(3,2) equals f(2,2). (See Fig. 9c), and during the coupling of a (2,1) mode with a (1,1) mode, f(2,1) equals f(1,1). (See Fig. 13). The assumption of a toroidal rotation would readily explain the fact that the toroidal mode number n relates the two frequencies.

A physical argument that supports this observation is that tearing modes are essentially caused by local concentrations of the current density or by electrons drifting in the toroidal electric field. It is very likely that the mode structure will therefore drift in the same direction and with the same speed as the drift of the electrons that is producing it.

8. CONCLUSION

The discharges with a high energy content during Neutral Injection may be divided into two types.

The first type is characterized by large, long, and regular sawteeth caused by the (1,1) mode at the q=1 surface. This surface and also the

q=2 surface are relatively close to the outside of the plasma: at resp. ~5.5 and 9.5 cm. Inside the q=1 surface the electron heat losses can, when time averaged, be explained by the measured line radiation and the sawtooth disruptions (about 50% each).

The second type is characterized by increasingly longer and disappearing sawtooth disruptions. Therefore, the plasma losses are considerably less in comparison to the discharges of the first class. The plasma energy content is accordingly higher during the quiescent period. The rational surfaces appear to be closer to the plasma centre, especially after a localized disruption at the q=1.5 surface, which ends the quiescent period. Both, the q=1 and q=2 surface, are displaced ~2.5 cm inwards in comparison to the discharges of the first type. In particular, this brings the q=2 surface closer to the steep current density gradient. The resulting large (2,1) and often also (1,1) modes are then responsible for substantial plasma losses either through disruptions or more continuously by energy transport across the islands. At slightly lower values of the external rotational transform (t_0 from 0.23 to 0.19) major current disruptions caused by the (2,1) mode may occur.

The only difference in the discharge build-up between the two types is additional gas puffing with deuterium. The first type has a constant level of helium. The second type has deuterium added to it at the beginning of the injection by gas puffing. This apparently increases the beam energy deposition at the plasma edge, impeding the current constriction towards the plasma centre of the sawtooth internal disruptions.

The problems encountered with the (2,1) tearing mode proved to be clearly linked with the toroidal plasma current.
In the WENDELSTEIN VII stellarator several means to avoid the deleterious effects of the (2,1) mode are possible. Firstly, increasing the stellarator external rotational transform t_0 when decreasing the plasma current in order to keep the q=2 surface at the outside away from the current density gradients. Although then difficulties with a shearless rotational transform of the WENDELSTEIN VII stellarator might be encountered. Secondly, tailoring the beam deposition or the radiation loss radial profiles by carefull addition of various gasses, such as D_2 and Ne.

ACKNOWLEDGEMENTS

The authors are pleased to acknowledge the continuing support of the technical crew of WENDELSTEIN VII-A, and in particular, the invaluable assistance of Mr. D. Gonda in making the X-ray measurements.

REFERENCES

/1/ "Neutral Injection into the W VII-A Stellarator"
W VII-A Team, Neutral Injection Group, presented by H. Renner
Proc. 9th Europ.Conf.on Contr.Fusion and Plasma Phys., Vol.I,
Oxford 1979

/2/ "Computation of Heating Efficiencies and Deposition Profiles for Neutral Injection into Wendelstein VII-A Stellarator"
I.E. Faulkner, G.G. Lister, W. Ott, E. Speth, idem

/3/ "Second Order Abel Inversion with Allowance for Spatial Resolution"
P. Smeulders, IPP 2/240, August 1978

/4/ H. Wobig, private communication

/5/ "Soft X-Ray Fluxes as a Diagnostic for Hot Plasmas"
P. Smeulders, IPP 2/233, January 1979

/6/ "Magnetic 'Islandography' in Tokamaks"
I.D. Callen et al.
Proc. IAEA Innsbruck (1978), IAEA-CN-F-1-1

/7/ "MHD-Modes in the W VII-A Stellarator"
W VII-A Team, presented by A. Weller
Bull. APS Conf. 23, 834 (1978)

/8/ "Strucuture of Low Frequency Oscillations of the Disruptive Instability in the TFR Tokamak"
TFR Group, Fontenay Report
EUR-CEA-FC-833 (1977)

/9/ "Non-Uniform Rotation of Magnetic Islands in ALCATOR"
R.S. Granetz, I.H. Hutchinson, D.O.Overskei
Bull. APS Conf, Vol. 24, 8, Boston (1979)

/10/ "Behaviour of Discharges and Internal Disruptions in TFR"
TFR Group, presented by D. Launois
Proc. 7th Europ.Conf. on Contr.Fusion and Plasma Phys.,
Lausanne 1975, Vol. II, 4-13

/11/ "Dependence of the (2,1) Tearing Mode on the Stellarator Field in Wendelstein VII-A"
W VII-A Team, presented by R. Jaenicke
Proc. 9th Europ.Conf. on Contr. Fusion and Plasma Phys., Oxford, 1979, Vol. I

/12/ "Disruptions in the Stellarator W VII-A"
W VII-A Team, presented by P. Smeulders
Proc. IAEA Symposium on Current Disruptions in Toroidal Devices, Garching 1979, IPP 3/51

/13/ "Energy and Particle Confinement in the Ohmically Heated W VII-A Stellarator"
W VII-A Team, presented by H. Renner
Proc. 7th Int.Conf. on Plasma Physics and Contr.Nucl.Fusion Research, Innsbruck (1978), IAEA-CN-37-H-2

/14/ "Simulation of X-Ray Signals"
A. Weller, IPP 2/251, June 1980